Quaternary Science Reviews 276 (2022) 107279

Contents lists available at ScienceDirect

Quaternary Science Reviews

journal homepage: www.elsevier.com/locate/quascirev

Oceanographic and climatic influences on Trooz Glacier, Antarctica during the Holocene

Rebecca L. Totten [a, *], Adlai Nathanael Reuel Fonseca [a, 1], Julia Smith Wellner [b], Yuribia P. Munoz [b, 1], John B. Anderson [c], Thomas S. Tobin [a], Asmara A. Lehrmann [a]

[a] Department of Geological Sciences, University of Alabama, 2003 Bevill Building, 201 7th Street, Tuscaloosa, AL, 35487, USA
[b] Department of Earth and Atmospheric Sciences, University of Houston, 312 Science and Research Building 1, Houston, TX, 77204, USA
[c] Department of Earth, Environmental, and Planetary Sciences, Rice University, 6100 Main Street MS 126, Houston, TX, 77005, USA

ARTICLE INFO

Article history:
Received 25 April 2021
Received in revised form
29 October 2021
Accepted 7 November 2021
Available online 23 December 2021

Handling Editor: I Hendy

Keywords:
Diatoms
Stable isotopes
Glacial marine
Sedimentology
Circumpolar Deep Water

ABSTRACT

To evaluate the significance of recent widespread glacial recession in the Antarctic Peninsula, it is imperative to extend the limited instrumented record of glacier change with long sedimentary archives of the Holocene. Reconstructing glacial histories that capture the variability of environments in the Antarctic Peninsula will enable better constraint of ocean and climate forcings on regional glacial stability. Two sediment cores are analyzed from the 2007 *RV/IB N.B. Palmer* cruise to Collins Bay, the embayment immediately offshore Trooz Glacier on the Graham Land coast, and provide an archive to test controls on long-term stability of outlet glaciers in an open bay setting. Radiocarbon and Lead-210 (a short-lived radioisotope) age-depth models provide a timeline for Trooz Glacier behavior and associated oceanographic changes over the last 10,000 years.

Magnetic susceptibility, grain size, diatom assemblage, total organic carbon, nitrogen, and stable isotopes of organic carbon are utilized as proxies for changing glacial and ocean conditions. Outer Collins Bay deglaciated by ~10000 cal yr B.P. Diatom abundance and organic content signal productivity increase during further glacial recession from ~8900 to 6100 cal yr B.P., which coincided with upwelling of relatively warm Circumpolar Deep Water into the bay. High productivity, characterized by *Thalassiosira antarctica*-dominated diatom assemblages with prominence of *Fragilariopsis kerguelensis*, indicate open marine conditions with incursion of offshore currents into the bay from ~6100 to 760 cal yr B.P. A sharp decrease in organic content, diatom abundance, and grain size indicate more sea ice and ice-tongue/ice-canopy advance from ~760 to 240 cal yr B.P., when the floating ice canopy in outer Collins Bay retreated to near its present-day position and productivity increased. During the period of the 1950's to 1990's, Trooz Glacier was one of only two Antarctic Peninsula glaciers that advanced slightly. Over the Holocene, oceanographic forcing dominated the long-term stability of Trooz Glacier due to its open aspect, and it is unknown how Trooz Glacier will respond to continued influence of Circumpolar Deep Water in the future. Understanding ocean forcings on glacial stability, together with other local controls like drainage basin configuration and bay geometry, should help contextualize the modern retreat and improve prediction of glacial response to prevalent Circumpolar Deep Water circulation in this dynamic region.

Abbreviations: AP, Antarctic Peninsula; CDW, Circumpolar Deep Water; KC, Kasten Core; JPC, Jumbo Piston Core; JTC, Jumbo Trigger Core; ACC, Antarctic Circumpolar Current; MS, Magnetic Susceptibility; %TOC, Total Organic Carbon; %TN, Total Nitrogen; $\delta^{13}C$, Stable carbon isotopes; $\delta^{15}N$, Stable nitrogen isotopes; PCA, Principle Components Analysis; FCM, Fuzzy C-Means; CRS, Chaetoceros Resting Spores; ADA, Absolute Diatom Abundance; LGM, Last Glacial Maximum; MHCO, Mid Holocene Climatic Optimum; LIA, Little Ice Age; MCA, Medieval Climate Anomaly.

* Corresponding author.
E-mail addresses: rltotten@ua.edu (R.L. Totten), adlainrfonseca@gmail.com (A.N.R. Fonseca), jwellner@uh.edu (J.S. Wellner), yuribia.munoz@gmail.com (Y.P. Munoz), johna@rice.edu (J.B. Anderson), ttobin@ua.edu (T.S. Tobin), alehrmann@crimson.ua.edu (A.A. Lehrmann).
[1] Address at the time work was done.

https://doi.org/10.1016/j.quascirev.2021.107279
0277-3791/

1. Introduction

The Antarctic Peninsula (AP) is the northernmost region of Antarctica (Fig. 1) and warmed over 5 times faster than the global mean during the period of the 1950's to late 1990's (Houghton et al., 2001; Vaughan et al., 2003, 2013; Turner et al., 2005). Notably, ~90% of the AP glaciers retreated during this time (Cook et al., 2005, 2014). Cumulatively, the AP contributed 2.5 mm to sea-level rise from 1979 to 2017 (Rignot et al., 2019). The AP region is undergoing a cooler climate phase more recently (Turner et al., 2016), yet relatively warm ocean currents dominate much of the continental shelf, which can melt marine-terminating glaciers from below (Jenkins and Jacobs, 2008; Moffat et al., 2009). In fact, glacier recession across the western AP has been largely ascribed to melting of glacial fronts due to the intrusion of relatively warm Circumpolar Deep Water (CDW; Cook et al., 2016). On the other hand, several ice shelves that lie between the -5 °C and -9 °C mean annual isotherms have collapsed since the 1990's (highlighted in pink in Fig. 1), perhaps due to summer surface melt that penetrates crevasses and leads to collapse (Morris and Vaughan, 2003). Ice shelves south of the -9 °C isotherm are thought to be more stable due to lesser influence of surface meltwater production during the summer (Scambos et al., 2003, 2009; Vaughan et al., 2013). These changes reflect the sensitivity of glaciers in the AP to complex feedbacks between the ocean, the atmosphere, and the cryosphere, and several studies document multi-proxy evidence of past stability of AP glaciers during the Holocene (e.g., Smith et al., 1999a; Domack et al., 2001; Bentley and Hodgson, 2009; Milliken et al., 2009; Michalchuk et al., 2009; Minzoni et al., 2015; Christ et al., 2015; Kim et al., 2018; Wellner et al., 2019). With an understanding of these glacial dynamics, we aim to address the relative importance of atmospheric versus oceanographic controls on the stability of modern AP ice shelves and outlet glaciers. The context of the long-term Holocene climate history, as well as several records of ice-shelf expansion and collapse in the AP (Pudsey and Evans, 2001; Brachfeld et al., 2003; Gilbert and Domack, 2003; Domack et al., 2005; Bentley et al., 2005; Hodgson et al., 2006) further provide a frame of reference for modern glacial sensitivity in the western AP region.

Bays and fjords that drain tidewater glaciers are repositories of

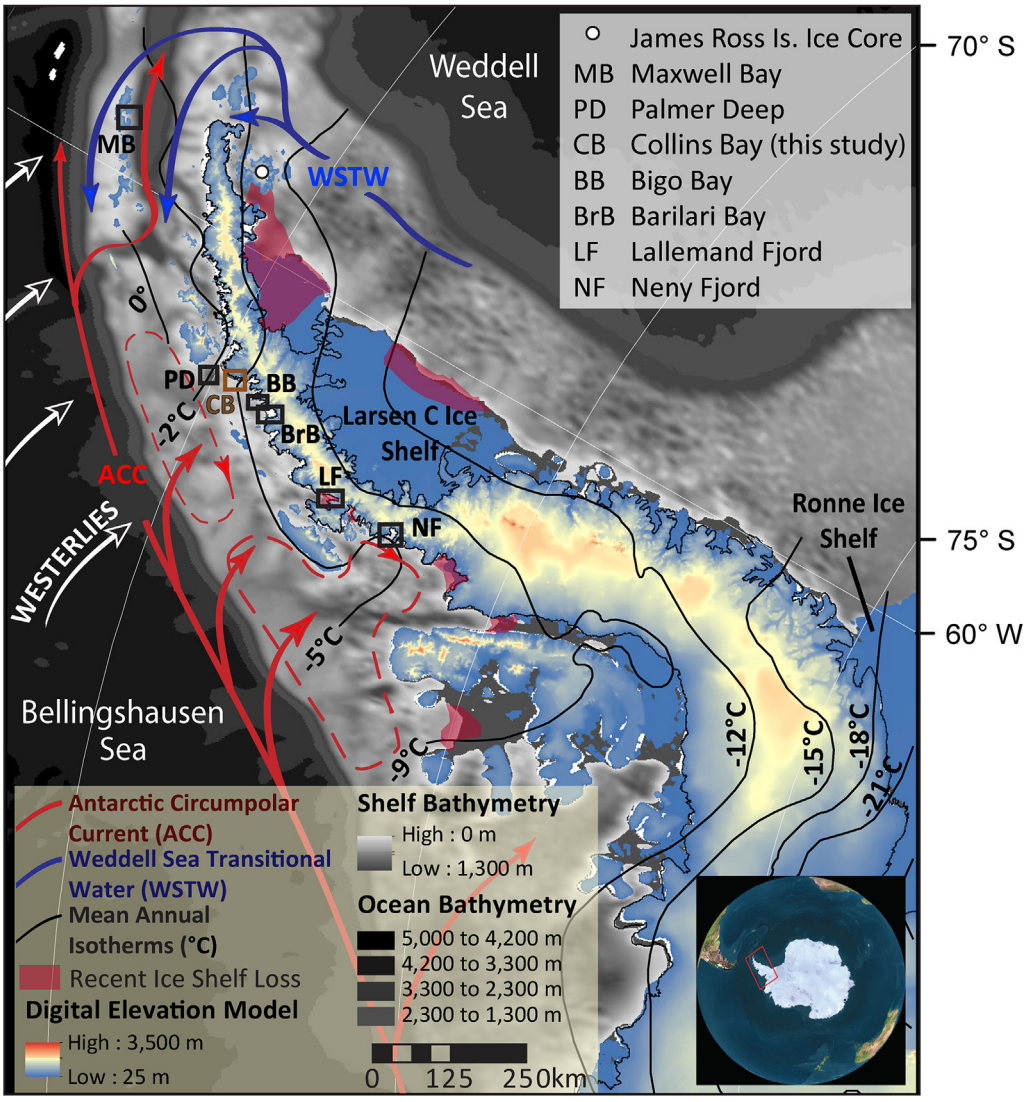

Fig. 1. Location of Collins Bay (CB) in the western Antarctic Peninsula. Collins Bay is compared with other western AP sites, including the Palmer Deep, Bigo Bay, Barilari Bay, Neny Fjord and Maxwell Bay. Modified from Minzoni et al. (2015, *QSR*, which includes information compiled from Landsat; NASA; GeoMapApp; Reynolds, 1981; Hofmann et al., 1996; Smith et al., 1999b; mean annual isotherms reported in Morris and Vaughan, 2003; Martinson et al., 2008).

sedimentary archives of climate and oceanographic change as glacial discharge is high in these drainage basins, and therefore are ideal for studying glacial sensitivity to past climate events (Griffith and Anderson, 1989). To test the controls on long-term AP glacial stability in relation to climatic and oceanographic changes, we reconstruct the Holocene history of Trooz Glacier from offshore sediments in Collins Bay, which is located on the Graham Land coast of the western AP where modified CDW is known to reach the coastline today (e.g., Jenkins and Jacobs, 2008; Cook et al., 2016). Sedimentology, sediment geochemistry, and diatom microfossil assemblage data from the well-preserved sedimentary archive of Collins Bay provide a record of Trooz Glacier stability throughout the Holocene. We compare Trooz Glacier history with a review of published glacier records from neighboring bays, fjords, and an over-deepened basin to elucidate controls on glacial response to climate variability in the western AP, providing a long-term context for its modern retreat. Specifically, we compare the record from Collins Bay which we define as an "open" bay setting, in which there is a large opening to the open ocean, with what we define as "restricted" fjord-type bays in which there is a smaller opening to the sea and an elongate, narrow geometry.

1.1. Climatic and oceanographic settings

Collins Bay (65°21′S, 64°3′W) is an open marine embayment draining Graham Land on the western AP, north of Beascochea Bay (Figs. 2 and 3) and 54 km southeast of the Palmer Deep, which is the location of one of the most expanded Holocene marine archives in the AP region (Domack et al., 2003). Collins Bay is a broad embayment (~5.6 km wide x ~9.5 km long), which differs from neighboring elongate, narrow fjords that have more restricted connections to the continental shelf. Collins Bay is largely occupied by glacial ice. As such, Trooz Glacier is more exposed to offshore circulation and water masses, providing an opportunity to contrast Collins Bay with more restricted fjords and their response to climate and oceanographic influence through time (Fig. 2).

The mean annual temperature of the Graham Land area is ~5 °C (Morris and Vaughan, 2003), and the melt bucket-averaged precipitation at Palmer Station (just north of Palmer Deep, Fig. 1) was 770 mm/yr between 1989 and 1997 (Turner et al., 2002). While precipitation data is sparse in the region, precipitation measured for Trooz Glacier in the 1980's was similar to Palmer Station at ~780 mm/yr (R. Mulvaney, personal comm. that was published Turner et al., 2002). Precipitation is relatively high in this area of the western AP due to net northwesterly flow of moist air over this region from the Bellingshausen Sea and depressions that track eastward, delivering most of the precipitation to coastal sites and creating a maritime climate (Turner et al., 2002).

Westerly winds drive the Southern Ocean around the continent towards the east, creating the Antarctic Circumpolar Current (ACC, Fig. 1), which drives modern ocean circulation as it links major ocean basins in the global ocean system (Convey et al., 2009). CDW is the main water mass of the ACC (Walker et al., 2007), and it mixes with shelf water to form modified Upper CDW, which is warmer than the shelf water and can flow into the near-shore regions of the AP (Convey et al., 2009; Cook and Vaughan, 2010; Pritchard et al., 2012). The presence of relatively warm Upper CDW (from now on referred to as CDW) on the western AP shelf increases basal melting of outlet glaciers and ice shelves (Ishman and Domack, 1994; Domack et al., 2003; Bentley and Hodgson, 2009; Hellmer et al., 2012; Pritchard et al., 2012) (Fig. 3). The relative warmth of the western AP seas contrasts with the eastern side of the AP, which is in the rain shadow of the AP mountains and is dominated by cooler, more saline Weddell Sea Transitional Water (e.g., Turner et al., 2002). Recent investigations north of James Ross Island, however, indicate that modified Upper CDW also influences the northeastern AP (Etourneau et al., 2019) and the Larsen Ice Shelf (Fig. 1), and may have led to long-term thinning of eastern AP ice shelves in the recent past as well, priming them for the instability and collapse observed in modern times (Domack et al., 2005; Wellner et al., 2019).

Using an extensive temperature and salinity dataset through World Ocean Database from 1945 to 2009, Cook et al. (2016) define three oceanographic regimes in the AP: 1) the south and west AP, which is dominated by CDW and overlain by Winter Water and Antarctic Surface Water; 2) the northeast AP, which is dominated by saline Shelf Water that is influenced by heat loss to the atmosphere and sea-ice production in the Weddell Sea; and 3) the Bransfield Strait of the northwest AP, which is a mixture of Shelf Water and modified CDW, also influenced by atmospheric and sea-ice interactions. Collins Bay is located at the southernmost tip of the third oceanographic regime, and is therefore under the influence of modified CDW, mixed with Shelf Water, and strongly influenced by sea-ice interactions (Fig. 1). By contrast to the southwestern CDW oceanographic regime, which averages 4 °C above the seawater freezing temperature—the Bransfield Strait regime averages 2 °C above seawater freezing temperature. The mean ocean temperature at >100-m water depth strongly influences glacier stability (Cook et al., 2016). Collins Bay is characterized by a mean annual temperature of 0.25 °C−1.25 °C from 100-m to 300-m water depth, respectively, thus placing it within the Bransfield oceanographic regime today.

1.2. Geologic and glacial settings

Collins Bay is the outlet for Trooz Glacier (Figs. 2 and 3). The glacier is 2.8 km-wide at its mouth and ~28 km-long. Trooz Glacier is located on the Kiev Peninsula, which is a predominantly ice-covered, oval-shaped peninsula projecting 35 km to the northwest from western Graham Land (Fig. 2). The drainage area of Trooz Glacier is ~580 km^2 with measured flow velocities up to 3 km/yr (Koppes et al., 2015). From 1956 to 1997, Trooz Glacier advanced 1.5 km, which was measured from satellite and aerial images by Cook and colleagues (2005; 2014). While almost all of the 860 glaciers of the AP retreated over this period, Trooz Glacier is one of only two marine-terminating glaciers in the AP that advanced >1 km (Cook et al., 2014). The percentage of Trooz Glacier size increase was less than 1%, however (Cook et al., 2014). Several glaciers within the northwestern AP (Bransfield Strait) oceanographic regime defined by Cook et al. (2016) have advanced more than 0.01%, however, from 1985 to 2004 C.E., while most glaciers in the northeast AP and the southern AP retreated.

The seafloor of the outer basin of Collins Bay (~10 km from the modern ice front) is characterized by rugged bedrock topography with sparse meltwater channels and small basins that were targeted for coring (Fig. 3). The outer basin has an area of 0.3 km^2 and is located approximately 10 km seaward of the Trooz Glacier terminus (Munoz and Wellner, 2018). The inner basin near the glacier terminus is ~2 km^2 (Munoz and Wellner, 2018).

The bathymetry of the western AP inner shelf is quite rugged and composed of glacially eroded bedrock that extends offshore into a relatively flat outer shelf that is underlain by a seaward dipping wedge of Neogene strata (Larter and Barker, 1989; Larter and Cunningham, 1993; Bart and Anderson, 1995; Rebesco et al., 1997; Smith and Anderson, 2010). The outer shelf is cut by several large troughs that contain elongate bedforms, including mega-scale glacial lineations, indicative of the troughs having been occupied by ice streams during the LGM (Heroy and Anderson, 2005, 2007; Wellner et al., 2006; O'Cofaigh et al., 2014; Larter et al., 2014; Lavoie et al., 2015). The glacially carved troughs

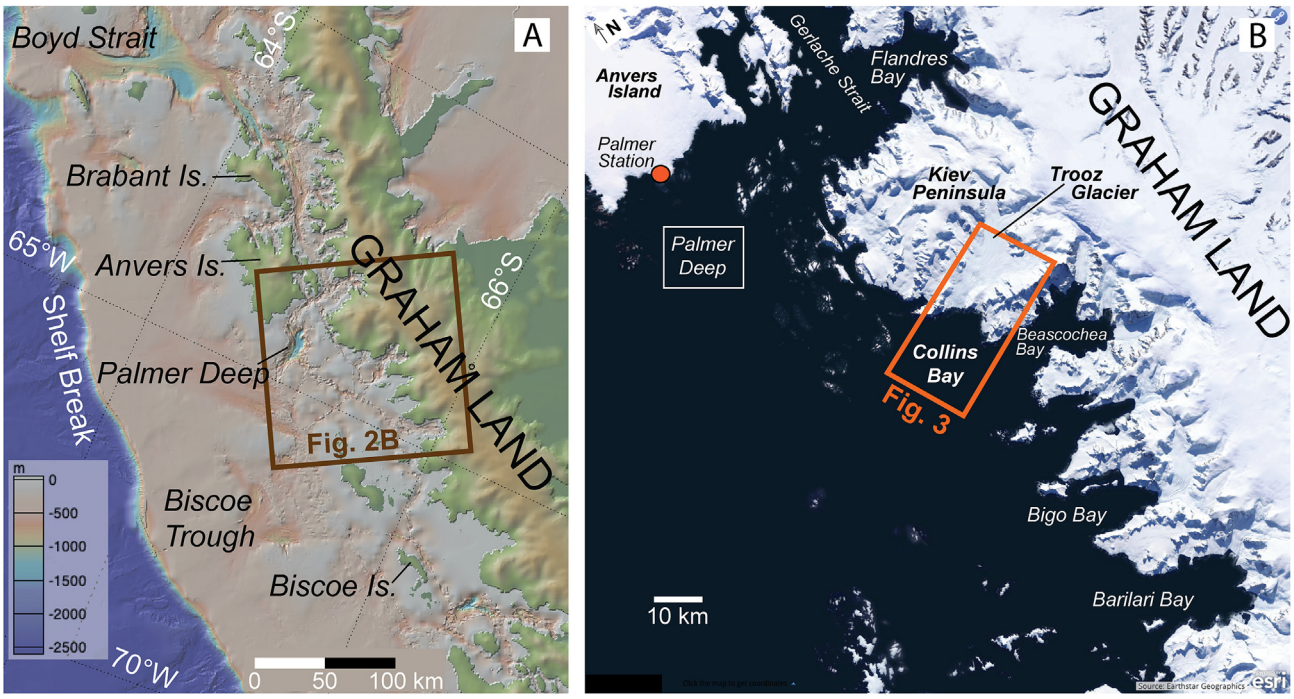

Fig. 2. On the Graham Land coast of the western Antarctic Peninsual (A), Trooz Glacier drains into the open marine Collins Bay (B). Maps constructed using bathymetry and digital elevation model in GeoMapApp (A) and the Polar Geospatial Center Rema Viewer (B).

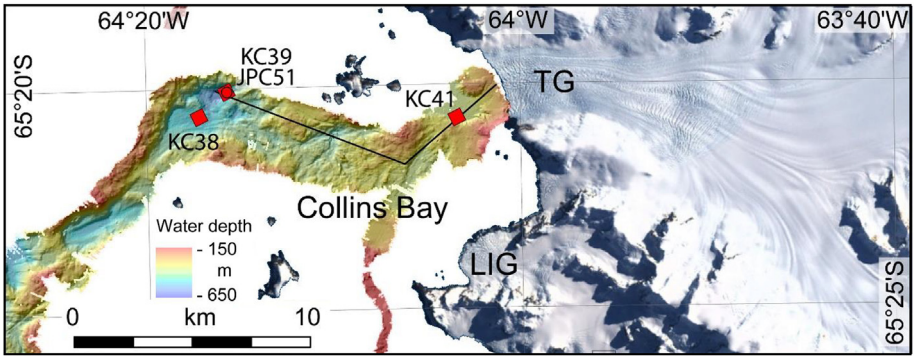

Fig. 3. Multi-beam swath bathymetry and location of sediment cores (red diamonds) collected from Collins Bay during the NBP0703 research cruise. TG: Trooz Glacier, LIG: Lind Glacier. Black line marks location of transect shown in Fig. 9. Modified from Munoz (2018). Satellite image from the Polar Geospatial Center. (For interpretation of the references to colour in this figure legend, the reader is referred to the Web version of this article.)

provide pathways for impinging CDW onto the continental shelf in the AP and in Amundsen Sea to the south, where CDW has been demonstrated to influence modern ice fronts (Fig. 1; e.g. Smith et al., 2017; Hogan et al., 2020).

The post-LGM retreat of individual ice streams from the AP continental shelf was rapid and episodic across the outer shelf of the western AP from ~17500 cal yr B.P. This was followed by recession from the middle shelf at ~14000 cal yr B.P. and to the inner shelf by 11000 cal yr B.P. (e.g., Heroy and Anderson, 2007; O'Cofaigh et al., 2014). As the Antarctic Peninsula Ice Sheet (APIS) receded onto the rugged bedrock topography of the inner shelf, drainage separated into many smaller outlets that experienced asynchronous glacial retreat to near their modern positions, ranging between 13000 and 7000 cal yr B.P. (Heroy and Anderson, 2007; O'Cofaigh et al., 2014; Lavoie et al., 2015). The variability in the timing of retreat from the inner continental shelf likely resulted from variable bathymetry, and implies that there were local controls on glacial stability, such as drainage basin configuration and bay geometry/aspect (Heroy and Anderson, 2005, 2007; O'Cofaigh et al., 2014; Minzoni, 2015).

Oceanographic influence on ice shelves and glaciers in West Antarctica has been recognized in Holocene marine sediment records (Hillenbrand et al., 2010, 2017; Peck et al., 2015; Minzoni et al., 2017; Smith et al., 2017), especially in the western AP where relatively warm CDW has been recorded on the shelf today, enhancing basal melt of ice shelves and outlet glaciers (Smith et al., 1999a; Smith and Klinck, 2002; Jenkins and Jacobs, 2008; Moffat et al., 2009; Cook et al., 2016; Wahlin et al., 2021). The mean annual temperature >100-m water depth is found to correlate highly with glacier change in the AP from 1945 to 2009 C.E. (Cook et al., 2016). It has further been suggested from high-resolution sediment records that high-latitude teleconnections, such as the El Niño–Southern Oscillation variability, may control or influence CDW incursion on the continental shelf, leading to ice-shelf loss in the last century (e.g., Smith et al., 2017).

2. Methods

Four sediment cores were collected from Collins Bay in 2007 during the *RV/IB Nathaniel B. Palmer* (NBP0703) cruise to the AP (Shipboard Scientific Party, 2007). Kasten core KC41, collected adjacent to the glacier front at 356 m water depth (Fig. 3), recovered 273 cm of watery, layered medium sand with silty clay, with minimal disturbance of the sediment-water interface. A Jumbo Piston Core (JPC51) from ~554 m water depth in the outer bay sampled recovered 13.64 m of interlayered olive gray silty clay and sand (Fig. 3), and a 1.33-m Jumbo Trigger Core (JTC51) was collected at the same time. Another 2.72-m core, KC39, was collected at the same site as JPC51, and a 2.50-m core KC38 was collected from the outermost basin in 501 m water depth (Fig. 3). Radiocarbon ages were obtained from KC41 and JPC51. A Lead-210 profile was collected from KC39. The combined ages from JPC51 and KC39 were used to produce a combined age-depth model (Table 1; Supplementary Data). Both the distal JPC51-KC39 core site and the more proximal KC41 results are used to reconstruct the timing of glacial and oceanographic changes in Collins Bay. Depositional environments and glacial marine conditions are investigated through interrogation of a large multi-proxy dataset, including: magnetic susceptibility (MS), grain size, total organic carbon (%TOC), total nitrogen (%TN), stable carbon and nitrogen isotopes ($\delta^{13}C$ and $\delta^{15}N$, respectively), and diatom assemblages. Variations in these environmental proxies are employed to interpret sedimentary environments and glacial conditions, as well as ocean temperature, productivity, and sea-ice concentrations at the sub-centennial scale over the last 10,000 years.

2.1. Chronology

Eight Radiocarbon (^{14}C, half-life of 5700 years) ages were obtained from calcareous foraminifera and shell fragments in NBP0703 JPC51 and KC41, which were analyzed by the National Ocean Sciences Accelerator Mass Spectrometry facility at the Woods Hole Oceanographic Institution (NOSAMS), the Accelerator Mass Spectrometry facility at the University of California-Irvine (UCIAMS), and the Institute for Particle Physics and Astrophysics at the Swiss Federal Institute of Technology (ETHZ) (Table 1). The radiocarbon ages were calibrated in the Calib v. 8.2 calibration software (Stuiver and Reimer, 1993, Stuiver et al., 2021). A radiocarbon reservoir correction of 500 ± 50 yrs was applied to the Marine20 curve which includes a global reservoir age of 600 yrs (Heaton et al., 2020) to produce a total reservoir age of 1100 ± 50 yrs, following the reservoir age corrections for Maxwell Bay (Milliken et al., 2009) and other bays of the Bransfield Strait Water oceanographic regime in the AP (Cook et al., 2016). These calibrated ages are reported in Table 2.

The Lead-210 (^{210}Pb, half-life of 23 years) activity was measured with a gamma detector every 2 cm of the upper sediment core NBP0703 KC39, which was collected at the same site as JPC51 (Figs. 3 and 4). Where the Lead-210 decay curve reaches a low, supported level at depth in the sediment column, the linear sedimentation rate can be calculated and used to assign ages to the known depths of the core samples. The Lead-210 ages from KC39 confirm good surface preservation and provide an average sedimentation rate of 4.14 mm/yr (0.414 cm/yr) for the upper core (Munoz, 2018). Therefore, the age of 43 cal yr B.P. (100 years before the time of collection at −57 cal yr B.P., or 2007 C.E.) was calculated at 41.4 cmbsf from sedimentation rate, and this age was included in the age-depth model, along with the surface age of −57 cal yr B.P.

We combined the uncalibrated radiocarbon ages from JPC51 and the two ages from the Lead-210 results to create an age-depth model using Bayesian statistics in the BACON Age Model software (an age-depth modelling software; Blaauw and Christen, 2011; Supplementary Data), which divides the cores into sections and estimates accumulation rates in the sections based on the ages. Again, we applied a total reservoir age of 1100 ± 50 yrs and used the Marine20 curve (Heaton et al., 2020) in the BACON software (Blaauw and Christen, 2011). We applied the same methodology to produce a BACON age-depth model in KC41 using the one radiocarbon age at its base. We apply the age-depth models to the core analysis in this study to interpret timing of environmental changes that are recorded in the sedimentological, geochemical, and paleontological proxy dataset.

2.2. Physical properties and sedimentology

KC41 and JPC51 were sampled every 20 cm for grain size, which was analyzed using a CILAS laser particle size analyzer at the University of Houston. The bulk sediment samples were dispersed in water with sodium hexametaphosphate to deflocculate clays and then transferred to the CILAS for grain size analysis following McCave et al. (1986). The Wentworth grain size classification (1922) was used to define sand, silt, and clay sizes.

MS and density were measured at the Florida State University Antarctic Research Facility using a Geotek Multi-sensor core logger at approximately 1-cm intervals throughout JPC51 and KC41. MS measures the amount to which materials can be magnetized - the more magnetic (or larger clastic and terrigenous) components there are in the sediment, the higher the readings. Low values correspond to a higher percentage of biogenic matter. MS can be used as a proxy to measure changes in the composition of the sediment which can be related to depositional processes. Density measures the mass content, which is related to the lithology and the compaction of the sediment.

2.3. Geochemical methods

Approximately 10 cc of bulk sediment was collected every 10 cm intervals in JPC51 and KC41. Carbonate was digested following the vaporous HCl decarbonation method (Komada et al., 2008) in order to remove the inorganic carbon. First, ~35 mg of the sediment from the samples collected were dried, crushed, and weighed into silver foil capsules following standard procedures (e.g., Komada et al., 2008), after which around 2–3 drops of organic-free Nanopure water were added to wet the samples and promote acidification (Harris et al., 2001). Samples were then placed in a glass desiccator adjacent to an open beaker of 25% HCl for 12–17 h, and then dried overnight prior to analysis. %TOC, %TN, $\delta^{15}N$, and $\delta^{13}C$ were measured with a Costech Elemental Analyzer (EA) and Thermo Delta V Mass Spectrometer operated under a continuous flow of ultra-pure He in the University of Alabama Stable Isotope Laboratory. Due to low organic content, the sediment samples were analyzed alongside a low-organic-content standard for every run using Elemental Microanalysis B2153, which has accepted measured values of 7.30‰ ± 0.13 for $\delta^{15}N$, 0.133% ± 0.023 for %TN, −26.66‰ ± 0.24 for $\delta^{13}C$ and 1.61% ± 0.09 for %TOC. Standard calibration and all carbon and nitrogen measurements are provided in the Supplementary Data.

2.4. Paleontological methods

Approximately 0.02 g of bulk sediment were sampled every 10 cm from both cores for absolute diatom abundance and assemblage analysis following the settling method (Fig. 4) (Scherer, 1994). Diatoms were counted at a 1000× magnification and identified to species level when possible (examples of observed diatom species are provided in Supplementary Data). Samples were first

Table 1
Sediment cores collected from Collins Bay (Fig. 3) and calibrated ages for NBP0703 KC39, KC41, JTC 51, and JPC51. Radiocarbon samples were analyzed in the UCIAMS, ETHZ and NOSAMS laboratories. Radiocarbon results were first calibrated in Calib 8.2 (Stuiver et al., 2021) with the Marine20 curve (Heaton et al., 2020) and a total reservoir correction of 1100 ± 50 yrs. The uncalibrated radiocarbon ages were then incorporated with the Lead-210 profile from KC39 (Fig. 4) in BACON age-depth modeling software (Bluaaw and Christen, 2011; see Supplementary Data). An age model for NBP0703 KC41 was also built in the BACON software using the basal radiocarbon age and a surface age assumption of −57 ± 1 cal yr B.P. (Supplementary Data).

Core ID N8P0703	Core Length (cm)	Latitude	Longitude	Water depth (m)	Core sample depth (cm)	Cumulative sample depth (cmbsf)	14C age (yr BP)	Age error (yr BP)	Calibrated age (cal yr BP) Marine20	Error (2 sigma)	Material sampled	Lab ID
KC38	250	−65.34406	−64.28649	501	n/a							
KC39	250	−65.33487	−64.26153	555	0	0			−57	1	Surface age assumption	
					41.4	41.4			43	20	Lead-210 (see Fig. 4)	
KC41	272	−65.34576	−64.05647	356	269–271	269–271	1870	65	762	381	Foraminifera	ETZH-65467
JTC51	133	−65.33484	−64.26152	554	n/a							
JPC51	1364	−65.33484	−64.26152	554	410	500	4560	20	3910	418	Shell fragment	UCIAMS-83303
					595–597	685–687	5410	20	5011	416	Foraminifera	NOSAMS-124898
					974–975	1064–1065	7020	70	6796	514	Foraminifera	ETZH-65460
					1217.5–1218	1307.5–1308	9000	45	8908	504	Shell fragment	ETZH-65461
					1221–1222	1311–1312	9110	60	9068	532	Shell fragment	ETZH-65465
					1301	1391	9855	25	10001	434	Scaphopod	UCIAMS-58872
					1360–1361	1450–1451	8830	85	8688	568	Foraminifera	NOSAMS-124897

counted at high-resolution (137 slides for JPC51 and 28 slides for KC41) across on 10 mm transect for *Chaetoceros* Resting Spores (CRS) abundance as a proxy for productivity. The second count, at 40 cm intervals, was for CRS-free assemblages to infer paleoenvironments from species that are sensitive to different conditions such as sea-ice concentration and temperature. Thirty-five slides of JPC51 were counted across 12 mm transects until a minimum of 400 non-CRS valves were tallied. Up to 5 transects were counted where non-CRS species abundances were low. Diatom slide counts were converted to absolute diatom abundance (ADA), expressed in diatom valves per gram of dry sediment (v/gds) using the equation from Scherer (1994) and Warnock and Scherer (2015):

$$\text{Absolute Diatom Abundance} = \left(no.\ of\ diatoms\ counted\ x\ beaker\ area\ in\ mm^2\right) \Big/ \left(no.\ of\ transects\ x\ transect\ area\ in\ mm^2\right) \Big/ \times (dry\ sediment\ mass\ in\ grams).$$

Only specimens with at least half of the valve preserved were counted. Diatom assemblages were then interpreted in the context of modern ecological preferences within the Southern Ocean, and statistically analyzed in assemblages using the multi-variate Principal Component Analysis (PCA) in the C2 Version 1.7 paleoclimate software (Juggins, 2007). PCA is used to depict the variability in the dataset and to evaluate the relative importance of each species. The ecological affinities of the diatom assemblages are used to interpret depositional processes and changing glacial marine environments, such as open marine, sea-ice, and ice-shelf or ice-canopy environments (following several precedents in the Southern Ocean, including Leventer et al., 1996; Stickley et al., 2005; Buffen et al., 2007; Pike et al., 2008; Allen et al., 2010; Minzoni et al., 2015). The diatom species percentages were also analyzed to group samples with similar assemblage composition using Fuzzy C-Means (FCM) analysis in the TACSWorks software suite (Gary et al., 2009) with a fuzzy exponent of 1.6, following methods in Minzoni et al. (2015). FCM is an especially valuable tool for paleoenvironmental analysis as it uses a soft-clustered matrix that relaxes the class exclusivity constraint and allows species to have memberships in more than one cluster (Bezdek, 1987; Bezdek and Pal, 1991), which is more characteristic of the natural environment. All diatom abundances and multi-variate results are provided in the Supplementary Data.

Table 2
A summary of each non-CRS diatom assemblage (DA) and non-CRS species composition, determined from the Fuzzy C-Means analysis (TACSWorks software; Gary et al., 2009).

Diatom Assemblage		Highest Species Membership
DA1	*Fragilariopsis curta* prominent	19.1% T1 15.4% *F. curta* 11.1% T2 8.5% *E. antarctica*
DA2	*Thalassiosira antarctica* dominant	24.8% T1 20.7% T2 10.9% *F. curta* 5.3% *T. ritscherii*
DA3	*Eucampia antarctica* prominent	20.7% T1 13.9% *E. antarctica* 12.7% *F. curta*

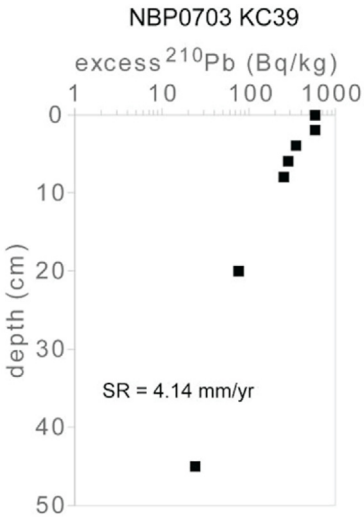

Fig. 4. Excess ^{210}Pb activity in Bequerels per kilogram (Bq/kg) in Kasten core NBP0703 KC39, which was collected from the same site as JPC51 and was used to constrain the age model of the upper sediment column. Sedimentation rate (SR) from Munoz (2018).

3. Results

3.1. Diatom abundance and assemblages

Diatoms are abundant in the sediments of Collins Bay and are well preserved throughout the sediment cores analyzed for this study (Figs. 5 and 6). CRS and total diatom (including non-CRS) abundances broadly follow the same trend, since CRS make up 70–90% of diatom assemblages in the AP (e.g. Allen et al., 2010). The basal unit of NBP0703 JPC51 is characterized by a low abundance of diatoms (~32 million v/gds of CRS). The diatom abundance increases up-section in the overlying unit where CRS abundance is ~129 million v/gds. The uppermost unit is characterized by relatively low CRS abundance, with an average of ~58 million v/gds.

The diatom species counts, performed every 40 cm in the core, were analyzed using PCA in the C2 v. 1.7 paleoclimate software to identify major axes that would explain the variability in the multivariate dataset and to gauge the relative importance of each species on the extracted axes (Fig. 7; Juggins, 2007; Supplementary Data). The first three axes have eigenvalues of 35.5%, 16.1% and 13.0% respectively, accounting for 64.6% of the total variability. The first two axes have the highest eigenvalues and account for the most significant assemblage transitions, and the Principle Component (PC) loadings help to identify trends in the diatom populations.

Three diatom assemblages (DA's) (Table 2) were defined by a second multi-variate statistical analysis defining fuzzy cluster memberships in the TACSWorks software (Gary et al., 2009; Supplementary Data), and these were ranked by most abundant species. *Thalassiosira antarctica*, which has two morphotypes T1 (cold) and T2 (warm), composed the greatest percentage membership of three DA's (background on diatom species is provided in section 4.2). The DA's, defined by percent membership of the most common diatoms within the assemblage, include: (**DA1**) the *Fragilariopsis*-prominent assemblage (15.4% *F. curta* with *T. antarctica* T1 at 19.1% and T2 at 11.1% of the membership); (**DA2**) the *Thalassiosira antarctica*-dominant assemblage (24.8% membership of *T. antarctica* T2, followed by 20.7% *T. antarctica* T1); and (**DA3**) the *Eucampia antarctica*-prominent assemblage (13.2% *E. antarctica*, 12.7% *F. curta*, 20.7% *T. antarctica* T1 and 11.3% *T. antarctica* T2).

3.2. Core NBP0703 JPC51 results

JPC51 is divided into five units based on lithology and variations in geochemistry and diatom assemblages: Unit 1 (1364–1261 cm core depth), Unit 2 (1261–810 cm), Unit 3 (810–704 cm), Unit 4 (704–390 cm), and Unit 5 (390–0 cm) (Fig. 5). The units were

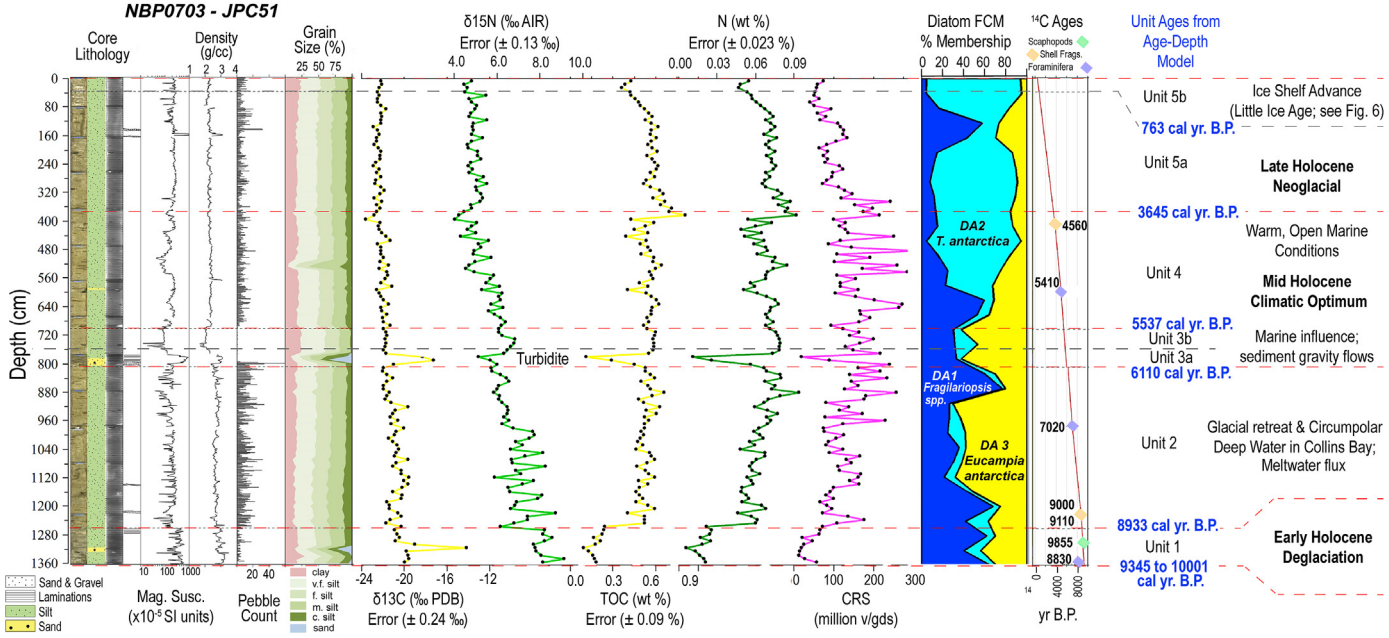

Fig. 5. Stratigraphic plot of key proxies used to interpret paleoenvironments in NBP0703 JPC51, including core lithology (core photographs, lithology, x-rays, and sedimentary structures) including magnetic susceptibility (Mag. Susc.); density; pebble count; grain size; stable isotopes of carbon (δ13C) and nitrogen (δ15N); total organic carbon (%TOC); total nitrogen (% TN); absolute abundance of Chaetoceros Resting Spores (CRS); and the Radiocarbon age model (uncalibrated dates on graph, with calibrated ages from the Age-Depth model at unit boundaries). Diatom Assemblages were determined by Fuzzy C-means (FCM) analysis in TACSWorks software and defined by % Membership (Gary et al., 2009). Elemental Analysis followed the methods of Komada et al. (2008; Supplementary Data).

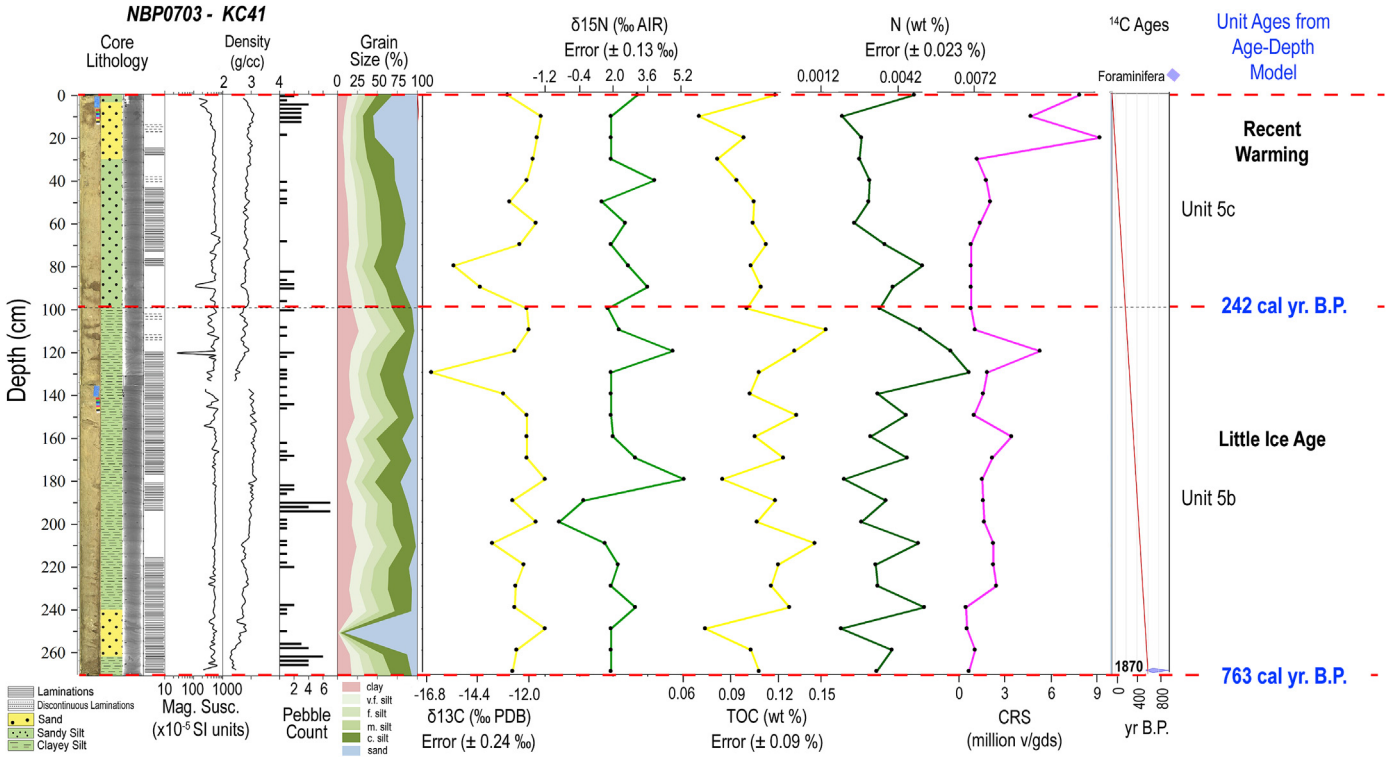

Fig. 6. Stratigraphic plot of key proxies used to interpret paleoenvironments in NBP0703 KC41, including core lithology (core photographs, lithology, x-rays, and sedimentary structures); including magnetic susceptibility (Mag. Susc.); density; pebble count; grain size; stable isotopes of carbon (δ13C) and nitrogen (δ15N); total organic carbon (%TOC); total nitrogen (% TN); absolute abundance of Chaetoceros Resting Spores (CRS) ; and the Radiocarbon age model (uncalibrated dates on graph, with calibrated ages from the Age-Depth model at unit boundaries). Diatom Assemblages were determined by Fuzzy C-means (FCM) analysis in TACSWorks software and defined by % Membership (Gary et al., 2009). Elemental Analysis followed the methods of Komada et al. (2008; Supplementary Data). The variability in carbon and nitrogen measurements are close to the error, and should be interpreted with caution.

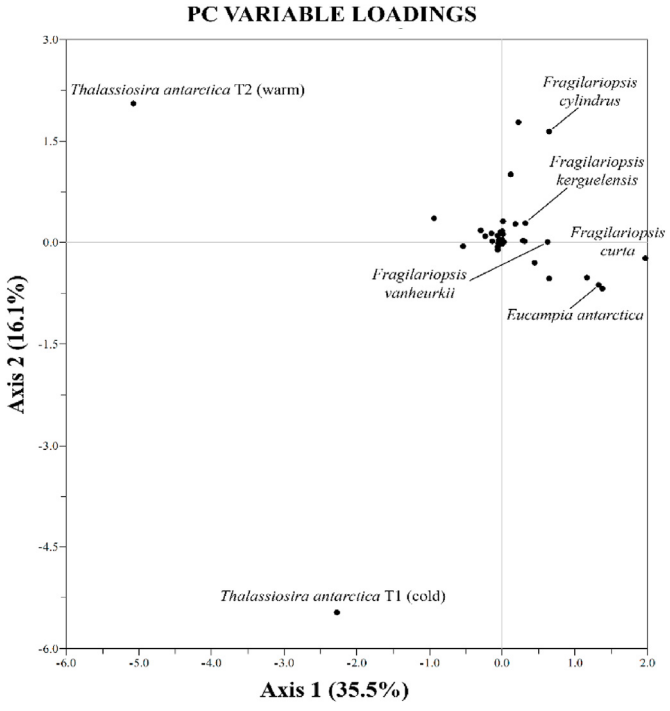

Fig. 7. Principal Component Analysis (PCA) results from Collins Bay JPC51 diatom counts. The ordination bi-plot with variable loadings is shown for Axes 1 and 2, with significant species variables labeled. PCA conducted with C2 Version 1.7 software (Juggins, 2007).

determined visually by lithology and trends in the multi-proxy datasets.

Unit 1 (1364–1261 cm core depth) is a dark gray (GLEY1 4/N) silt with scattered pebbles, infrequent laminations and sand. Sand percentages decrease up-section, from 20% to <1% with a prominent sand layer of about 10 cm thickness at 1300 cm core depth (Fig. 5). Both magnetic susceptibility (MS) and density are high in this unit (1364–1261 cm), compared to the rest of the core. $\delta^{15}N$ ranges from ~6 to 9‰, and $\delta^{13}C$ ranges from −19.5 to −20.5‰ in Unit 1, with the exception of a sand layer at 1300 cm with a $\delta^{13}C$ value of ~ −14‰. The %TN and %TOC are low throughout the unit at ~0.02% and 0.3% respectively. Diatoms are sparse with mainly *E. antarctica* (primary member of DA3) and *F. curta* (primary member of DA1) present. CRS diatom abundance is ~10 million v/gds.

Unit 2 (1261–810 cm core depth) is a dark greenish gray (GLEY1 4/1) to olive gray (5Y, 5/2) silt (Fig. 5). Pebbles are abundant throughout the unit and 2 gravel layers are present at 1150- and 1220-cm core depth. Sand percentages average < 1%, but the coarser silt component (32–63 μm) decreases up-section. The transition from Unit 1 to Unit 2 is marked by an increase in %TOC from 0.2 to 0.6 and %TN from 0.02 to 0.07% above which it is constant, apart from small peaks between 800 and 900 cm $\delta^{15}N$ and $\delta^{13}C$ decrease gradually up-section in Unit 2. CRS abundance generally increases up-section in this unit, ranging between 80 and 270 million v/gds. *E. antarctica* is the dominant species and the *Eucampia antarctica*-dominant DA3 is the primary diatom assemblage in Unit 2.

Unit 3 (810–704 cm core depth) is characterized by a dark greenish gray (GLEY1 4/1) to very dark gray (GLEY1 3/1) silt (Fig. 5).

Sand percentages are generally <1% but reach up to 36% in the laminated section (810–760 cm). Pebbles are absent in upper Unit 3 (from 780 to 704 cm), yet abundant in lower Unit 3 (from 810 to 780 cm), which is a criterion for subdividing Unit 3 into Unit 3b (no pebbles) and Unit 3a (abundant pebbles). Unit 3a is a fining upward sand-gravel sequence with an erosive contact at the base. Pebbles lie at 810-cm core depth with a coarse-grained sediment layer overlying it followed by laminated sediment just above it at 770-cm core depth. %TOC, %TN, and $\delta^{15}N$ record low values while $\delta^{13}C$, MS, and density show an increase at the sand layer between 810 cm and 780 cm in Unit 3a. CRS abundance in the sand layer in Unit 3a is ~10 million v/gds. Unit 3b is comparatively finer with only silt. %TOC, % TN, and $\delta^{15}N$ increases up-section, while $\delta^{13}C$, MS and density decrease up-section. CRS abundance spans between 120 and 180 million v/gds. *E. antarctica* and *F. curta* are still the most prominent species and *T. antarctica* (the primary member of DA2) becoming more abundant up-section in Unit 3.

Unit 4 (704–390 cm core depth) is primarily composed of an olive gray (5Y 5/2) to dark greenish gray (GLEY1 4/1) silt (Fig. 5). A few sand grains (<1%) are at 590 cmbsf, and pebbles are abundant throughout the unit. $\delta^{15}N$ and $\delta^{13}C$ gradually decrease up-section, but %TN and %TOC have similar values as Unit 3b. CRS abundance ranges between 80 and 250 million v/gds. DA2 is the most prominent assemblage in this unit and *T. antarctica* is again the most abundant species.

Unit 5a (390–40 cm core depth) is an olive gray (5Y 5/2) to dark greenish gray (GLEY1 4/1) silt (Fig. 5). Pebbles are abundant throughout, and 2 gravel layers lie at ~150 cm core depth. %TOC and %TN values gradually decrease, and $\delta^{15}N$ and δ^{13} values remain relatively constant, ranging from 4.0 to 5.5‰ and from −23.5 to −21.5‰, respectively. CRS abundance is relatively low, ranging between 80 and 130 million v/gds. Both DA1 and DA2 are the dominant assemblages with *T. antarctica, F. curta,* and *Fragilariopsis vanheurkii* being the predominant species in Unit 5a.

Uppermost Unit 5b (40–0 cm core depth), is an olive gray (5Y 5/2) silt with few sand grains (<1%) and scattered pebbles (Fig. 5). Density is relatively low ~2.2 g/cc. MS, $\delta^{15}N$, %TOC and %TN record relatively low values but gradually increase up-section to 20 cm core depth while $\delta^{13}C$ is relatively constant throughout. $\delta^{15}N$ is slightly lower than the underlying unit, with values from ~4.5 to 5.0‰. CRS abundance is ~50 million v/gds. DA2 and *T. antarctica* dominate Unit 5b.

3.3. Core NBP0703 KC41 results

Two units are identified in KC41 based on lithology: Unit 5b (272–100 cm core depth), which is characterized by finer grain size than Unit 5c (100–0 cm) (Fig. 6).

The lower unit in KC41 (271–100 cm), equivalent to Unit 5b in JPC51, is composed of greenish gray (GLEY1 5/1) clayey silt with few small pebbles and laminations throughout (Fig. 6). Sand percentage varies between 4 and 91%, but are, on average, lower than the overlying subunit 5c (14% compared to 27%). MS and density are relatively constant throughout the unit, with the exception of a decrease in MS and slight increase in density at 120 cm $\delta^{15}N$ and $\delta^{13}C$ range from~-0.5 to 5.3 and from −16.5 to −11.2‰, respectively, which is much lower than in JPC 51. %TN and %TOC are both an order of magnitude lower in KC41 than in JPC 51. The %TOC increases at 120 cm and %TN decreases. The CRS abundance is relatively low in this unit at ~2 million v/gds. CRS abundance peaks at 120 cm core depth (to ~4 million v/gds) along with %TN and $\delta^{15}N$, which are noticeably higher than the rest of the unit.

The overlying subunit, Unit 5c (100–0 cm core depth), is greenish gray (GLEY1 5/1) sandy silt with laminations present throughout (Fig. 6). Sand varies between 7 and 53% and increases up-section, followed by a decrease at the core top (the upper 10 cm). Pebbles are abundant in the upper 30 cm. MS and density values remain relatively uniform throughout this unit. %TOC and % TN values decrease up-section, followed by an increase in the core top. $\delta^{15}N$ varies, and $\delta^{13}C$ generally increases up-section, followed by a decrease at the core top. CRS abundance is ~1 million v/gds from 100- to 30-cm core depth, above which they increase to ~8 million v/gds towards the core top.

3.4. Combined sediment core chronology

Eight radiocarbon samples are reported in Table 1 (first reported in Munoz, 2018). The age model for NBP0703 KC41 was constrained from a single radiocarbon age of 1870 ± 65 radiocarbon yr. B.P. near its base, collected from foraminifera from 269- to 271-cm core depth. NBP0703 JPC51 over-penetrated the sediment-water interface, so the age model of that site was produced by combining the seven radiocarbon ages from JPC51 with the Lead-210 age model of a Kasten core taken at the same site, KC39 (Fig. 4), which had good recovery of the sediment-water interface and the upper 90 cm of the sediment column (Supplementary Data). The base of JPC51, at 1360-1361-cm core depth, dates to 8830 ± 85 radiocarbon yr B.P. from calcareous foraminifera, and three additional dates from ~1301, ~1222, and ~1218 cm yield slightly older ages (ranging from 9855 ± 25 to 9000 ± 45 radiocarbon yr B.P.; Table 1). The significantly older age at 1217.5–1218.5 cm core depth is interpreted to be reworked and an outlier in the BACON age-depth model (Table 1; Supplementary Data). Overlying ages in JPC51 include: 7020 ± 70, 5410 ± 20, 4560 ± 20 radiocarbon yr B.P., taken from 974-975-cm, 596-597-cm, and 410-cm core depth, respectively.

The combined BACON age-model for NBP0703 JPC51 and KC39 (Supplementary Data), as well as the linear age model from a single radiocarbon age in KC41, which was taken from a more proximal site within Collins Bay, are used to mark the timing of lithologic unit boundaries that represent significant glacial and oceanographic changes and events. Unit 1 spans from 9345 ± 402.5 to 8933 ± 504 cal yr B.P. Unit 2 spans 8933 ± 504 to 6110 ± 338.5 cal yr B.P. Unit 3 spans 6110 ± 338.5 to 5537 ± 306 cal yr B.P. Unit 4 spans 5537 ± 306 to 3645 ± 304.5 cal yr B.P., and Unit 5 spans 3645 ± 304.5 cal yr B.P. to when the core was collected in 2007 CE, or −57 cal yr B.P., which is also recorded in the trigger core of JPC51, which is JTC51. NBP0703 KC41 also includes calibrated age ranges within Unit 5, including most of subunit 5b ranging from 764 ± 191.5 cal yr B.P. to 242 ± 100 cal yr B.P., and includes another upper subunit 5c, ranging from 242 ± 100 cal yr B.P. to when the core was collected in 2007 CE, or −57 cal yr B.P.

4. Discussion

4.1. Regional comparison of Holocene glacial marine records

Here we compare the multi-proxy dataset from Collins Bay with the IODP Leg 178 Site 1098 in the Palmer Deep (Figs. 1, 2 and 8), a seminal Pleistocene to Holocene paleoclimate record for the AP (Domack et al., 2001) and the Southern Ocean. Comparisons are also made among cores from different bays and fjords along the western AP shelf that have long and comparable multi-proxy records of glacial history, productivity, and hydrographic change (Fig. 8).

The Palmer Deep is an isolated basin on the inner continental shelf, located south of Anvers Island and just 54 km to the northwest of Collins Bay (Fig. 2). Proxy records from the high-accumulation, high-resolution sediment record from the Palmer Deep (Leventer et al., 1996; Domack et al., 2001; Taylor and Sjunneskog, 2002; Maddison et al., 2005) have been used to

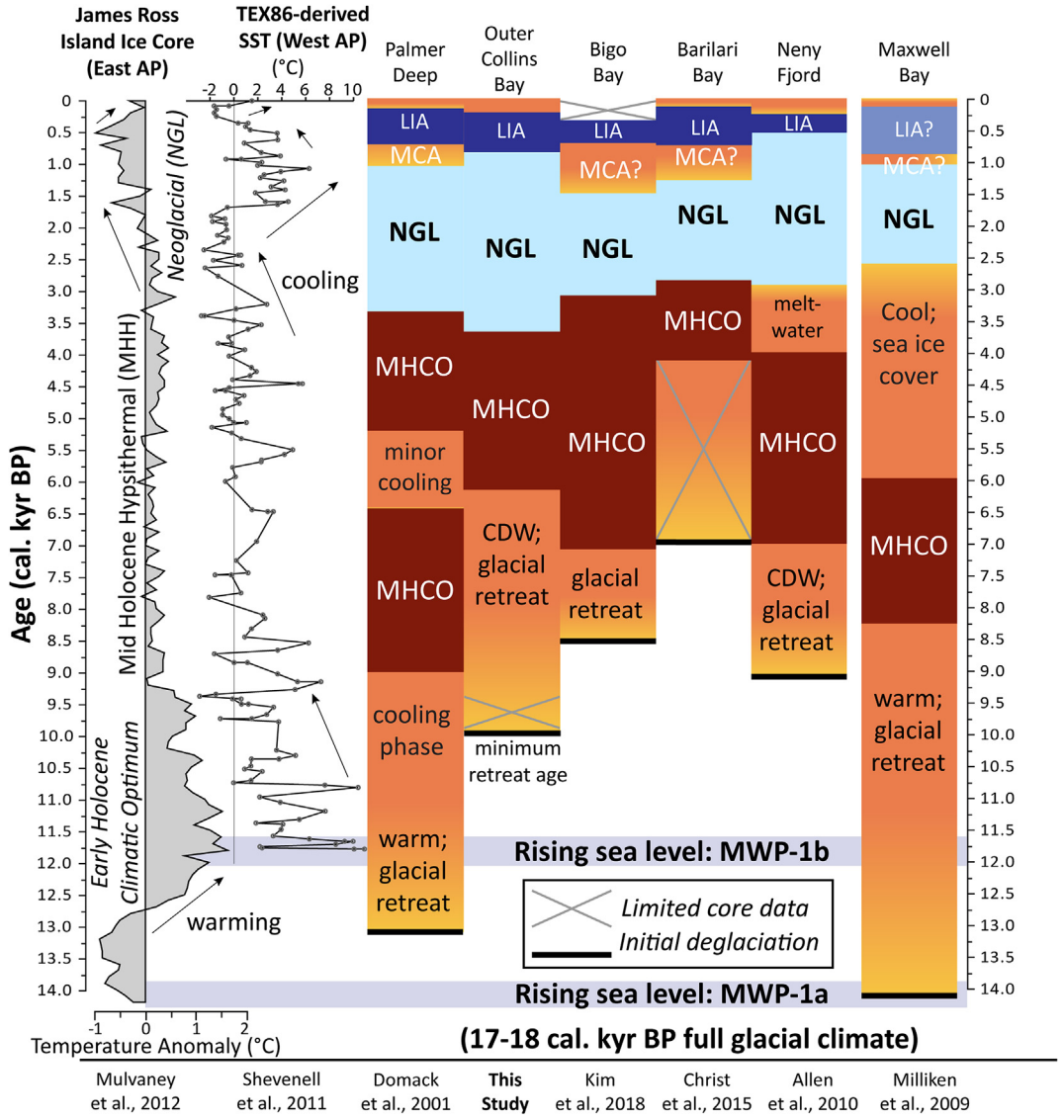

Fig. 8. Comparison of western Antarctic Peninsula marine records of glacial history during the Holocene. The ice core temperature record from James Ross Island (Fig. 1; Mulvaney et al., 2012) is used to compare climate events with the glacial marine environmental history during the Holocene. Additionally, a sea surface temperature (SST) record from the Palmer Deep (Shevenell et al., 2011) provides further comparison of oceanographic changes which may be related to glacial behavior. Each column represents an individual site, and each box denotes the duration of glacimarine response to climate events. LIA—Little Ice Age; MCA—Medieval Climate Anomaly; NGL—Neoglacial; MHCO—Mid Holocene Climatic Optimum (modified from Minzoni, 2015).

characterize the paleoenvironmental evolution of the western AP during the Holocene, including the following events: LGM (older than 13180 cal yr B.P.), deglaciation (13180-11460 cal yr B.P.), a climatic reversal (11460-9070 cal yr B.P.), the Mid Holocene Climatic Optimum (MHCO; 9070-3360 cal yr B.P.), the Neoglacial (3360-100 cal yr B.P.), and the Little Ice Age (LIA; 700-100 cal yr B.P.; Fig. 8). The Palmer Deep does not capture the variability of western AP climate changes, however, and therefore marine records throughout the region are compared.

We compare the Collins Bay record with the ~14,000-yr record from Maxwell Bay in the South Shetland Islands (Milliken et al., 2009, Fig. 8), not only due to its long and extensive multi-proxy record, but also because it represents a more temperate environment in the northernmost AP that is low relief (Turner et al., 2002; Milliken et al., 2009) and has both a wide main opening and another minor inlet today, likely making it sensitive to oceanographic influences of the Bransfield Strait (Fig. 1). We further compare our results with those from fjords that are narrow, shallow, and restricted to the open ocean (with elongated geometries and <600 m water depth) on the Graham Land coast and have similarly long records of Holocene glacial marine evolution: Bigo Bay, located 27 km south of Collins Bay (Kim et al., 2018) and Barilari Bay, located 45 km south of Collins Bay (Figs. 1 and 2; Christ et al., 2015). Both Bigo Bay and Barilari Bay are elongated bays that directly face the Bellingshausen Sea and do not have prominent islands to the west of their openings, much like Collins Bay. We further compare the Holocene multi-proxy record from Collins Bay to that of Neny Fjord (Allen et al., 2010), which is located ~350 km south of Collins Bay (Fig. 1). Neny Fjord is a polar fjord and is known to be influenced by modified CDW circulating in Marguerite Bay today (Smith and Klinck, 2002; Moffat et al., 2009).

4.2. Environmental interpretations from diatom assemblage (DA)

Key to the reconstruction of Collins Bay glacial history and that of each study site in our comparison are diatom assemblages preserved within the core sediment. In this study, the environmental significance of Diatom Assemblages (DAs) is interpreted in the context of modern ecological affinities of diatom species in the Southern Ocean (summarized in Table 2). The DA1 *Fragilariopsis*-prominent assemblage (15.4% *F. curta* with *T. antarctica* T1-cold at 19.1% and T2-warm at 11.1% of the membership) is interpreted to be the result of greater concentration of sea ice in Collins Bay, as *F. curta* is known for its strong sea-ice affinity in the Southern Ocean (e.g., Zielinski and Gersonde, 1997; Armand et al., 2005; Gersonde et al., 2005; Buffen et al., 2007; Pike et al., 2009). *F. curta* and another species in this assemblage, *Fragilariopsis cylindrus*, can also be epibenthic within sea-ice communities, and are found in ice-edge water, in melted sea-ice and associated surface water (Garrison et al., 1987; Garrison, 1991; Scott et al., 1994; Leventer and Dunbar, 1996; Armand et al., 2005; Pike et al., 2008). It has been suggested that *F. curta* may seed in the water column from fast ice during spring sea ice recession and is found in summer sea-ice too (Leventer and Dunbar, 1996; Taylor et al., 1997; Cunningham and Leventer, 1998).

By contrast, *T. antarctica* is associated with seasonally open waters and has two morphotypes: T1, which is associated with cold water masses, often found as sea ice is forming during late summer and autumn, and T2, which is the warm variety, common in warmer water masses and in open ocean-type environments with a well-mixed water column (Taylor et al., 2001; Taylor and Sjunneskog, 2002; Domack et al., 2003; Crosta et al., 2005). The second assemblage, the DA2 *Thalassiosira antarctica*-dominant assemblage (24.8% membership of *T. antarctica* T2-warm, followed by 20.7% *T. antarctica* T1-cold), therefore is interpreted to signify seasonally open conditions in Collins Bay, with variable sea surface temperature. *T. antarctica* composed the greatest percentage of all the non-CRS counts throughout the core, supporting the interpretation that Collins Bay remained open to the Bellingshausen Sea through most of the Holocene.

The third assemblage, DA3 *Eucampia antarctica*-prominent assemblage (13.2% *E. antarctica*, 12.7% *F. curta*, 20.7% *T. antarctica* T1-cold and 11.3% *T. antarctica* T2-warm), is interpreted to be indicative of sea-ice cover or an ice shelf/tongue, and in some cases including advection of offshore material to the sub-ice-shelf environment. *E. antarctica* has been associated with iron-fertilization, and associated with melting icebergs (Burckle, 1984; Armand et al., 2008; Conway et al., 2016), which may indicate periods of meltwater emanating from the glacier that leads to a bloom of *E. antarctica*. The resting spores of *E. antarctica* are robust and have been further interpreted as a proxy for current winnowing and reworking when they are abundant and other species are absent or sparse (Truesdale and Kellogg, 1979; Taylor et al., 1997; Cunningham and Leventer, 1998). When the robust *E. antarctica* resting spores sink in the water column, they may be advected by offshore currents into the sub-ice shelf/sea-ice covered area.

We discuss the relative membership of DA's (Table 2) within each interval to facilitate interpretation of environmental conditions in Collins Bay through the Holocene.

4.3. Deglaciation of Collins Bay after the LGM

During the LGM, the APIS extended to the continental shelf break of the western AP (Bentley and Anderson, 1998; Heroy and Anderson, 2005; Wellner et al., 2006; Heroy and Anderson, 2007; O'Cofaigh et al., 2014; Lavoie et al., 2015). Based on their LGM ice sheet reconstruction, Bentley and Anderson (1998) suggest that the ice sheet would have been on the order of a kilometer thick in the vicinity of Collins Bay based on grounding depths in inner shelf basins. The APIS receded from the outer shelf to a mid-shelf location ~14000 cal yr B.P., followed by highly diachronous grounding line retreat from the rugged inner shelf after ~11000 cal yr B.P. (Heroy and Anderson, 2005; O'Cofaigh et al., 2014). There is an overall pattern in which the initiation of grounding line retreat occurred later from north to south along the AP. Maxwell Bay in the South Shetland Islands began to deglaciate ~14200 cal yr B.P. (Milliken et al., 2009), and Palmer Deep experienced deglaciation between 13180 and 9070 cal yr B.P. (Domack et al., 2001). Embayments along the southern Graham Land coast, including Bigo Bay and Barilari Bay, began to deglaciate around 8500 cal yr B.P. and 7022 cal yr B.P., respectively (Christ et al., 2015) and Neny Fjord in Marguerite Bay deglaciated between 9090 and 7000 cal yr B.P. (Allen et al., 2010). This overall latitudinal trend in the timing of deglaciation is expected given differences in shelf and bay bathymetry, size and hypsometry of glacial drainage basins, local climate, and oceanography.

Our results from Collins Bay are generally consistent with the regional patterns of deglaciation for the AP. The oldest radiocarbon ages from the base of NBP0703 JPC51, range from 10001 to 8688 cal yr B.P., and—including the potentially reworked age of 10001 ± 434 cal yr B.P. at 1301 cmbsf (Table 1) that would have originated in an earlier marine phase of the bay—are consistent with deglaciation occurring by the Early Holocene (Fig. 9). The oldest unit of NBP0703 JPC51, Unit 1, in outer Collins Bay ranges from 9345 ± 402.5 to 8933 ± 504 cal yr B.P. based on the BACON age-depth model (Fig. 5; Supplementary Data). The presence of sand, pebbles, relatively high values of MS and density indicate terrestrial components that were delivered to the basin under proximal glacial marine conditions when the grounding line of Trooz Glacier extended to outer Collins Bay (Figs. 5 and 9). The $\delta^{15}N$ and $\delta^{13}C$ values are high in Unit 1, and–together with the other proxy indicators of terrestrial influence–we interpret this to indicate a lack of marine organic source and greater terrestrial input at this time. Terrestrial inputs may include ancient lithified organics, but mostly likely include very little organics in the granitic source area of Graham Land–indicating that the lack of marine productivity is the main control on stable isotope composition of the sediment. The sand layer at 1320 to 1300 cm in core JPC51 is likely the result of sediment gravity flow(s) and is characterized by the lowest TOC and highest $\delta^{13}C$ values (0.09%; −14.172‰; Fig. 5; Supplementary Data) in the core, which is consistent with a terrestrial source. Overall low %TN and %TOC values confirm terrestrial influence with little marine productivity during this time (Fig. 5). An anomalously old age of 10001 ± 434 cal yr B.P. (Table 1; Fig. 5). is interpreted as reworked, which is common in proximal glacimarine deposits–yet its presence indicates marine conditions that require a habitable sea floor in Collins Bay during the Early Holocene. Low CRS diatom abundance further confirm low productivity in Unit 1, which is also characterized by both the *Fragilariopsis*-prominent DA1 and the *Eucampia antarctica*-dominant DA3, an assemblage that has been associated with sub-ice shelf (or sub-ice canopy) conditions in which advection of offshore currents carry phytoplankton under the floating ice, dissolving all but the most robust valves such as *E. antarctica* (e.g., as interpreted in Minzoni et al., 2015). *E. antarctica* resting spores are robust, and when found in high abundance, they may indicate current winnowing and reworking because they are dissolution resistant, much like *F. kerguelensis* (Truesdale and Kellogg, 1979; Taylor et al., 1997; Cunningham and Leventer, 1998). Therefore, Unit 1 documents the last phase of retreat of the APIS from the continental shelf and into Collins Bay during the Early Holocene, when an extended Trooz Glacier remained grounded in the bay, likely with a floating ice

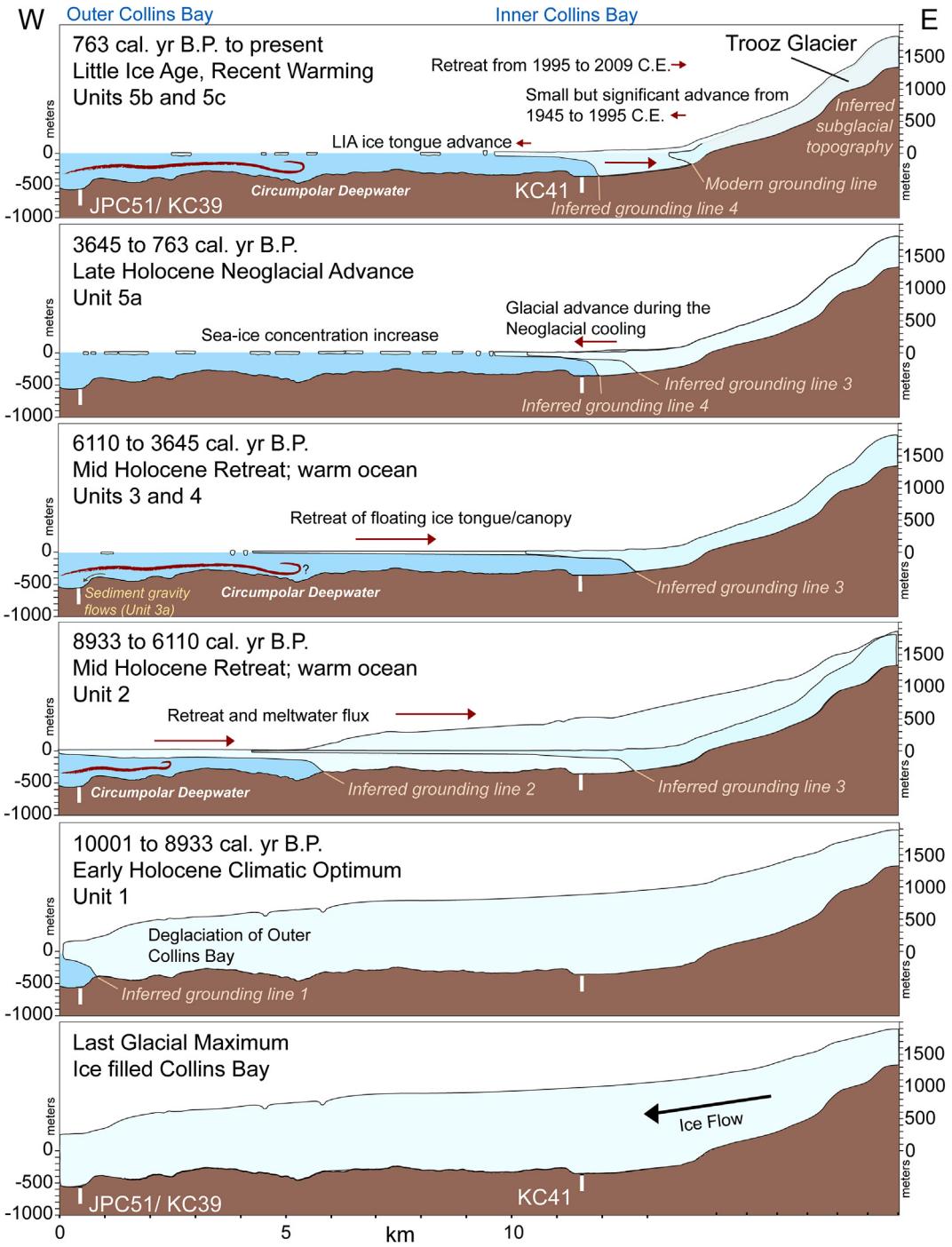

Fig. 9. Interpretation of glacial retreat in Collins Bay from the Last Glacial Maximum to present (cross section location in Fig. 3). Brown: bedrock, gray: ice, blue: water (modified from Munoz, 2018). Model constructed using data from the Polar Geospatial Center and Bedmap2 (Fretwell et al., 2013). A <1% increase in the areal extent of Trooz Glacier was observed from 1945 to 1995 (Cook et al., 2014) and retreat from 1995 to 2009 C.E. (Cook et al., 2016). (For interpretation of the references to colour in this figure legend, the reader is referred to the Web version of this article.)

tongue or canopy of ice at its terminus (Fig. 9). The rapid Early Holocene retreat of the ice sheet from the continental shelf in the area is consistent with ice-sheet reconstructions that are based on geological data (e.g., Heroy and Anderson, 2007; O'Cofaigh et al., 2014) and with results from geophysical modeling (Jamieson et al., 2014).

4.4. Glacial retreat and CDW in Collins Bay (8933–6110 cal yr B.P.)

The overlying Unit 2 in JPC51 spans 8933 ± 504 to 6110 ± 338.5 cal yr B.P. and is characterized by silt with an abundance of pebbles throughout the unit, including gravel layers near the base of the unit (Fig. 5). Unit 2 exhibits little variability in grain size throughout the unit, indicating that sedimentary processes varied little over the time of its deposition. The high and increasing

%TN and %TOC values indicate an abrupt initiation of marine productivity at the base of Unit 2, followed by steady increase as Collins Bay deglaciated. The $\delta^{13}C$ values decrease to ~ −20‰ at the base of Unit 2, indicating marine phytoplankton source, likely due to a decrease in ice-shelf cover, which facilitated photosynthesis in the upper water column. The *E. antarctica*-dominant DA3 dominates Unit 2, with both *E. antarctica* and *F. curta* as the dominant species, which are diatoms with sea-ice affinity. *E. antarctica* is associated with meltwater-released nutrients like iron, phosphorous, and silica which are limiting to phytoplankton in the Southern Ocean (Burckle, 1984; Arrigo et al., 2003; Coale et al., 2003; Armand et al., 2008; Gerringa et al., 2012; Conway et al., 2016). *Fragilariopsis kerguelensis* is an open marine species that is also abundant in Unit 2 and has been associated with relatively warm CDW in Neny Fjord to the south (e.g., Allen et al., 2010). The presence of *F. kerguelensis*, therefore, suggests that warm CDW impinged onto the western AP continental shelf during the Mid Holocene (8933–6110 cal yr B.P.) and likely came in contact with the seaward extent of Trooz Glacier in Collins Bay (Fig. 9). $\delta^{13}C$ continues to decrease while total diatom abundance and CRS abundance increase, reflecting rising productivity and onset of seasonally open marine conditions from 8933 to 6110 cal yr B.P. Furthermore, bulk $\delta^{15}N$, which has been interpreted to record nitrate utilization in the surface water of marine settings (Francois et al., 1992; Altabet and Francois, 1994), decreased at this time, indicating that diatoms, which were demonstrated to be the dominant phytoplankton that regulate surface water productivity in Bigo Bay just to the south, likely increased productivity in response to upwelling of nutrient-rich CDW (Kim et al., 2018 and references therein). Therefore, we interpret that Trooz Glacier retreated and opened outer Collins Bay to incursions of CDW during the Early and Mid Holocene, and meltwater flux from Trooz Glacier was high during this interval, leading to *E. antarctica* blooms (Figs. 5 and 9).

The Early and Mid Holocene retreat of Trooz Glacier and deglaciation of outer Collins Bay coincide with widespread climate amelioration in the AP, documented in peak atmospheric temperatures from ice core proxy records on James Ross Island (Mulvaney et al., 2012) and several other marine records (e.g., Bentley et al., 2009) and terrestrial lake records (e.g., Ingolfsson, et al., 1998). These observations are also consistent with sedimentary records from the western AP that include evidence for warm CDW incursion onto the continental shelf at this time (Domack et al., 2001; Leventer et al., 2002; Allen et al., 2010; Milliken et al., 2009; Christ et al., 2015; Peck et al., 2015; Kim et al., 2018). For example, Neny Fjord records evidence of CDW from 9000 to 7000 cal yr B.P. (Fig. 8; Allen et al., 2010), with relatively warm oceanic species *F. kerguelensis* and *Thalassiossira letiginosa* associated with intrusions of CDW in Marguerite Bay, which have been observed and modeled more recently by Smith and Klinck (2002) and Moffat et al. (2009). CDW is above freezing, and if it comes in contact with outlet glaciers, can cause basal melting, increasing ablation rates and contributing to glacial retreat (e.g., Smith and Klinck, 2002; Jenkins and Jacobs, 2008 and several others). Therefore, CDW appears to have been prevalent in the western AP from ~9000 to 6000 cal yr B.P. and was most likely a major contributor to glacial retreat, not just in Collins Bay and Neny Fjord, but across the western AP at this time, including the George VI Ice Shelf (Fig. 1; Bentley et al., 2009). CDW incursion has also been interpreted as the driver of glacial retreat in Bigo Bay and Barilari Bay at 8500 and 7000 cal yr B.P., respectively (Figs. 1 and 8; Christ et al., 2015; Kim et al., 2018). Shevenell et al. (2011) suggest that SST in the Palmer Deep area may have been as much as 10 °C higher than today in the Early Holocene and remained high, yet variable, until finally decreasing after ~8000 cal yr B.P. (Fig. 8). This warmth could be related to the Early Holocene Climatic Optimum evident in ice core atmospheric temperatures (Mulvaney et al., 2012), but the prolonged warmth in an open marine site was likely influenced by warm oceanic water flowing onto the shelf and changing the overall hydrography (Fig. 1). Therefore, the glacial evolution at this time may be related to both CDW influence and a relatively warm climate.

4.5. The Mid-Holocene Climatic Optimum (6110–3645 cal yr B.P.)

Unit 3, a dark greenish gray silt, records pelagic deposition in a distal, open marine setting from 6110 ± 338.5 to 5537 ± 306 cal yr B.P. based on the BACON age-depth model (Fig. 5; Supplementary Data). Lack of pebbles, low productivity, and low CRS abundance with high $\delta^{13}C$ values in a prominent sand layer (Unit 3a) is interpreted as the deposit of a low-density turbidity current, which often travel several kilometers along the seafloor. The turbidite is characterized by a fining-upward sequence with laminations overlying a sand layer and pebbles. The normal grading of Unit 3a, coupled with the presence of *E. antarctica* and DA3 as the dominant assemblage, suggests meltwater and glacial retreat, which release nutrients that may cause diatom blooms, especially of *E. antarctica* (see discussion in section 4.4; (Burckle, 1984; Arrigo et al., 2003; Coale et al., 2003; Armand et al., 2008; Gerringa et al., 2012; Conway et al., 2016).

Higher total diatom abundance with a lower $\delta^{13}C$ value in Unit 3b implies high phytoplankton productivity and warm marine conditions (Fig. 5). *F. curta* and *F. vanheurkii* are the predominant species in Unit 3b, suggesting the presence of sea ice; however, a noticeable increase in *T. antarctica* suggests that there is more marine influence, perhaps due to greater seasonal variability. *F. kerguelensis* is abundant in Unit 3b and, in combination with lowering bulk $\delta^{15}N$ and thus higher nitrogen utilization at the top of the unit (Francois et al., 1992; Altabet and Francois, 1994; Kim et al., 2018), still indicates the influence of the warm CDW incursion, resulting in elevated productivity from the upwelling of deeper, nutrient-rich water, in Collins Bay.

Unit 4 spans 5537 ± 306 to 3645 ± 304.5 cal yr B.P. and is composed of mostly silt with a thin sand layer and abundant pebbles (Fig. 5). Productivity trends are of similar values to that of Unit 3 and gradual decrease in $\delta^{15}N$ and $\delta^{13}C$ suggest continued open marine conditions with elevated marine phytoplankton productivity and CDW influence. From 540- to 500-cm core depth (4603–4355 cal yr B.P.), the presence of well sorted silt with no sand, low MS, and high diatom abundance is evidence for moderate glacial meltwater flux during this time, possibly due to prolonged influence of CDW that would have led to significant basal melting of the floating ice tongue/canopy that extended offshore of Trooz Glacier (Fig. 9). The short-lived spike in the CRS diatoms at this interval may be due to meltwater-released elements from the glacier that caused a diatom bloom. The trends in Unit 4 are consistent with the warm conditions of the Mid Holocene Climatic Optimum (MHCO), which occurred between 9070 and 3360 cal yr B.P. in Palmer Deep (Domack et al., 2001), between 7000 and 2800 cal yr B.P. in Neny Fjord to the south (Allen et al., 2010), and between 8200 and 2600 cal yr B.P. in Maxwell Bay to the north (Milliken et al., 2009, Fig. 8). The MHCO was also expressed from 7060 to 3060 cal yr B.P. in Bigo Bay, an embayment directly to the south of Collins Bay on the Graham Land coast that was also influenced by CDW at this time (Fig. 8; Kim et al., 2018).

4.6. The Late Holocene Neoglacial (3645–763 cal yr B.P.)

Unit 5a spans 3645 ± 304.5 to 763 ± 347 cal yr B.P. and is interpreted as silt deposited in open marine conditions, which include the transition to cooler conditions during the Neoglacial, a climate event that is marked by a cooling trend in both ice cores and

SST records of the western AP starting ~3000 cal yr B.P. (Figs. 5 and 8; Shevenell et al., 2011; Mulvaney et al., 2012). Values of %TOC, %TN and CRS abundance are high near the base of Unit 5b and decrease up-section, which indicates the transition from the warm, open marine conditions of the MHCO to the cool Neoglacial. $\delta^{15}N$ and $\delta^{13}C$ values are consistent with abundant marine phytoplankton and suggest continued marine influence in Collins Bay during the Late Holocene cooling. *T. antarctica*-dominant DA2 is the prominent assemblage in the base of Unit 5, while the top of Unit 5a is characterized by *Fragilariopsis*-prominent DA1 and an increase in pebble abundance, indicating calving and ice-rafting into the bay. The dominance of the *Fragilariopsis*-prominent DA1 with *F. curta and F. vanheurkii* strongly implies enhanced sea-ice cover in outer Collins Bay during the Late Holocene. The offshore diatom *F. kerguelensis* is sparse in Unit 5a and 5b, further suggesting that CDW incursion into Collins Bay weakened during this time of prevalent sea-ice conditions. We therefore interpret relatively low bulk $\delta^{15}N$ during the Late Holocene to be the result of nitrate utilization due to enhanced stratification from greater meltwater flux, either due to seasonal sea-ice melt, as was interpreted at this time by Kim et al. (2018) in Bigo Bay to the south, or due to increased meltwater from an advanced ice shelf calving front, as was interpreted by Christ et al. (2015).

Many regions on the AP have experienced a cooling event interpreted as the Neoglacial at different times: Maxwell Bay at ~2600 cal yr B.P. (Milliken et al., 2009), Bigo Bay at 3060 cal yr B.P. (Kim et al., 2018), Barilari Bay at 2815 cal yr B.P. (Christ et al., 2015), Neny Fjord at 2800 cal yr B.P (Allen et al., 2010). and the Palmer Deep at 3360 cal yr B.P. (Domack et al., 2001, Fig. 8). Therefore, the Neoglacial period was expressed in Collins Bay nearly 500 years before the Palmer Deep and one-thousand years before Barilari Bay and Neny Fjord to the south. While the Neoglacial event was driven by atmospheric cooling, this early expression of cooling conditions in Collins Bay may be due in large part to the absence of CDW, which exerts greater influence on open marine settings than restricted fjords like Barilari Bay or Neny Fjord (Figs. 1 and 2).

4.6.1. The Medieval Climatic Anomaly (~1700 cal yr B.P.)

The Medieval Climatic Anomaly (MCA; Lamb, 1965; Grove and Switsur, 1994) is an event that is usually distinguished by enhanced productivity under open marine conditions in glacial marine settings (e.g., Minzoni et al., 2015; Kim et al., 2018), with a core period of 950 to 750 cal yr B.P. (Lüning et al., 2019). The MCA has been recognized in a few locations along the AP (Fig. 8), with onset ~1600 cal yr B.P. in the northern Bransfield Basin (Barnard et al., 2014), ~1250 cal yr B.P. in Herbert Sound in the eastern AP (Minzoni et al., 2015), ~1000 cal yr B.P. in Maxwell Bay (Milliken et al., 2009), ~1150 in the Palmer Deep (Domack et al., 2003), and ~1460 cal yr B.P. in Bigo Bay (Kim et al., 2018, Fig. 8). In Barilari Bay, $\delta^{13}C$ increased from 1325 to 625 cal yr B.P., but there was no strong evidence for the MCA event (Christ et al., 2015). We also lack strong evidence to support the occurrence of the MCA in Collins Bay. There is no appreciable increase in productivity proxies in NBP0703 JPC51 Unit 5a that we can interpret as the MCA. The increase in pebbles at 170 cmbsf in NBP0703 JPC51 could be the result of a warming event that led to enhanced calving and basal melting, resulting in greater ice-rafted debris delivery to the seafloor—but ice-rafting is also prevalent during times of glacial advance. Further study, including high-resolution sampling of paleo-temperature proxies, is required to determine whether the MCA was expressed in Collins Bay, and regional comparison should elucidate controls on the expression of this climate event in the Southern Hemisphere (Lüning et al., 2019).

4.7. The Little Ice Age (763–242 cal yr B.P.)

The MCA was followed by cooling during the Little Ice Age (LIA), which has been documented in several ice cores of West Antarctica from 750 to 0 cal yr B.P. (see comparison in Stenni et al., 2017 and references therein), with varying expression and timing in inner shelf embayments of the AP (Minzoni, 2015). Unit 5b in NBP0703 JPC51 dates to 763 ± 347 cal yr B.P., and is characterized by low $\delta^{15}N$ and $\delta^{13}C$ values and low productivity (Fig. 5). Absolute diatom abundance and CRS abundance are also low compared to rest of the core, and the *T. antarctica*-dominant DA2 is the dominant assemblage with significant percentages of the robust diatom species *E. antarctica*, whose presence may suggest advection of ocean water masses into the bay (following interpretations of Domack et al., 2001; Pudsey and Evans, 2001; Domack et al., 2005; Minzoni et al., 2015). The proxy evidence collectively suggests the presence of an ice tongue or ice canopy in the outer bay and cool conditions.

The proximal core NBP0703 KC41 was collected just 2 km from the modern Trooz Glacier ice front (Fig. 3), and the core correlates to the uppermost Unit 5b of JPC 51 and comprises an additional subunit, 5c (Fig. 6). The basal subunit of KC 41 (Unit 5b) spans from 764 ± 191.5 to 242 ± 100 cal yr B.P. (Fig. 6; Table 1; Supplementary Data). The $\delta^{13}C$ values are high (~- 12.6‰), due to proximity to the glacial front and low marine phytoplankton productivity near that site. The $\delta^{13}C$ in JPC51, by contrast, is ~ −20‰, which indicates marine phytoplankton source of organics (Fig. 5; Supplementary Data). Furthermore, bulk $\delta^{15}N$ is low, and along with low %TOC, %TN and CRS abundance, implies less marine organic matter production. In general, the productivity-related environmental proxies are much lower in KC41 than in JPC51, and this is likely due to proximity to the grounding line of Trooz Glacier. It is typical for productivity to be muted by high sediment flux in the proximal glacial marine setting; high sand concentration and pebbles, including sediment gravity flow deposits, are characteristic of environments proximal to the grounding line. We interpret these combined proxy data (high sand content, pebbles, and low organic content) to indicate greater proximity to the glacier front, and advance in the inner bay from 763 to 242 cal yr B.P. (Fig. 9). This timing corresponds to the Little Ice Age (LIA), which is also recorded in outer Collins Bay by NBP0703 JPC51, and is distinguished by characteristically low TOC and low productivity. The LIA has been identified in a several locations around the AP, often resulting in ice-shelf or ice-tongue advance, as was first demonstrated for the Müller Ice Shelf in Lallemand Fjord to the south of Collins Bay (Figs. 1 and 8; Domack et al., 1995; Shevenell et al., 1996). The LIA was also identified in the Palmer Deep from 700 to 100 cal yr B.P. (Domack et al., 2001), in Bigo Bay from 680 to 280 cal yr B.P. (Kim et al., 2018), in Barilari Bay at 730 to 82 cal yr B.P. (Christ et al., 2015), and in Maxwell Bay at 850 to 140 cal yr B.P (Milliken et al., 2009; Majewski et al., 2012; Simms et al., 2012). Thus, the glacial expression and timing of the LIA was much more synchronous than any prior Holocene climatic event in the western AP.

4.8. Recent warming (242 cal yr B.P. to present)

An increase in the CRS abundance in uppermost Unit 5c in KC41, accompanied by an increase in pebbles and sand (Fig. 6), suggests a proximal glacial marine depositional environment during ice retreat from the inner bay, leading to the warmer marine conditions observed in Collins Bay today. Low MS values at the top of the core are likely related to higher biogenic input (as was also interpreted in Neny Fjord by Allen et al., 2010). The onset of recent warming in Collins Bay is earlier than the timing of Palmer Deep ~100 cal yr B.P. (Domack et al., 2001), Maxwell Bay ~140 cal yr B.P.,

Bigo Bay ~280 cal yr B.P. (Kim et al., 2018), and Barilari Bay, which began warming 82 cal yr B.P. (Christ et al., 2015). We note that from the instrumented period of 1956–1997 C.E., however, Trooz Glacier experienced a net glacial advance of 1.5 km (Cook et al., 2014). With a relatively large drainage basin, it is possible that Trooz Glacier advanced during this recent period of warming due to greater accumulation, likely sourced from the Westerlies (Turner et al., 2002; Thomas et al., 2017). Trooz Glacier is one of only two marine-terminating glaciers in the AP that advanced >1 km during this time (out of 860 defined glaciers in the region), yet the percentage of Trooz Glacier drainage basin size change was quite minimal, with less than 1% increase (Cook et al., 2014). It is important to note that these observations are limited to spatial extent, and extent of the glacier does not necessarily capture other internal dynamics, which may result from acceleration and thinning, for example. With such a small net area change, we are cautious to interpret the significance of the Trooz Glacier advance during the period of recent rapid warming that took place from the 1950's to the 1990's (following Cook et al., 2014). Since 1995 C.E., the AP climate has undergone a slight cooling (Turner et al., 2016), and the Trooz Glacier terminus has retreated >0.01% per year, supporting the interpretation that modified CDW incursion, which may vary with time, is the key factor influencing the stability of glaciers along the western and southern AP (Cook et al., 2016). Trooz Glacier and Collins Bay are located at the boundary between two oceanographic regimes, which have different variants of CDW as it is modified through Shelf Water and sea-ice interactions (Cook et al., 2016). The boundary between Bransfield Strait Water-dominated and CDW-dominated oceanographic regimes may also vary with time, and since Collins Bay is at the boundary, it should be significantly impacted by this variation.

The evidence for widespread retreat is overwhelming in the AP, with ~90% of glaciers that have shrunk in size in from the 1950's to the 1990's (Cook et al., 2005, 2014). The unprecedented synchronicity of modern warming in these disparate fjords and embayments strongly suggests a common forcing, which may include modern atmospheric warming and prevalence of relatively warm CDW in the AP region. More recently, the widespread recession of glaciers in the southwestern and northeastern AP has been largely attributed to incursions of warm CDW, with glacier changes strongly correlated to ocean temperatures >100-m depth (Cook et al., 2016). Further decadal-scale resolution analyses of core tops with short-lived isotope age models are needed to more precisely date and characterize the onset of the recent rapid warming in sediment archives of the AP, so that we may compare forcings of the last century upon glacial stability and oceanographic conditions in these embayments. Trooz Glacier should be included in such an analysis because it is one of the only glaciers in which a slight advance was observed during this time (Cook et al., 2014), and more finely resolved analysis of NBP0703 KC41 can help explain which factors may have led to its apparent stability during modern times.

4.9. Forcings on glacial behavior

Trooz Glacier in Collins Bay began its retreat much earlier than Bigo Bay (Kim et al., 2018) and Barilari Bay (Christ et al., 2015), which are located just south of Collins Bay and in a similar climatic and oceanographic setting (Figs. 1 and 2; Turner et al., 2002; Cook et al., 2016). However, Bigo Bay and Barilari Bay both continued to experience deglaciation that resulted in an absence of glacial ice in these bays today versus more extensive glacial ice cover in Collins Bay. All three bays are facing the Bellingshausen Sea without protection of a nearby island (Figs. 1 and 2). The difference in retreat timing (Fig. 8), therefore, may be directly related to the bay geometry and drainage basin configuration. Collins Bay is a loosely defined embayment and may be more susceptible to oceanographic influence, in contrast with Bigo Bay and Barilari Bay, which are both elongated and more confined fjord-type bays. Collins Bay is fed by one large glacier, Trooz Glacier, whereas Bigo Bay and Barilari Bay are fed by multiple small glaciers (Fig. 2), which have less glacial ice contribution and may respond more rapidly to ocean and climate warming, as evidenced by their modern retreat (Cook et al., 2014). This begs the question of whether Collins Bay has undergone the same level of retreat as the smaller glaciers that feed Bigo Bay and Barilari Bay to the south. One can extrapolate that if Trooz Glacier were to recede, multiple small outlet glaciers would feed a larger, more defined bay setting, similar to its neighbors. Therefore, Collins Bay is not fully deglaciated; while Bigo Bay and Barilari Bay underwent early retreat, Collins Bay is still covered in floating ice and may or may not have retreated and re-advanced during the Little Ice Age. This may be the reason why, in part, Trooz Glacier advanced slightly during the period of recent rapid warming from the 1950's to the 1990's, while almost every other marine-terminating glacier in the AP retreated (Cook et al., 2005, 2014). A strong oceanographic forcing and air-sea-ice interaction may also be the reason for advance of Trooz Glacier, since Collins Bay sits within the southernmost extent of the Bransfield Strait Water-dominated oceanographic regime, while Bigo Bay and Barilari Bay sit within the northernmost extent of the CDW-dominated oceanographic regime, defined by Cook et al. (2016). The Bransfield Strait Water averages 2 °C above the freezing point of seawater, whereas the southwestern AP region is dominated by less modified CDW that averages 4 °C above the freezing point of seawater. This difference in average water temperature, especially below 100-m depth, may be a key reason for the difference between Trooz Glacier and the neighboring bays just to the south. The front of CDW-dominated oceanographic regime may have shifted over recent decades, explaining why Trooz Glacier has more recently retreated >0.01% from the 1995–2009 C.E. (Cook et al., 2016).

During sea-level rise and climate amelioration after the LGM, Collins Bay retreated much later than the Palmer Deep despite their close proximity (54 km) to one another (Fig. 1; Domack et al., 2001). An obvious distinguishing factor between the two sites is the relative proximity of core sites to glacial fronts and relative position on the continental shelf. Collins Bay is directly fed by Trooz Glacier, whereas the Palmer Deep is a deep marine basin in an open location on the continental shelf. Based upon its depth and location, we expect that the Palmer Deep would experience retreat much sooner than any inner shelf embayments. Glaciers in Maxwell Bay retreated ~14,000 cal yr B.P. (Milliken et al., 2009), however, and is an embayment of the South Shetland Islands in the northern-most tip of Antarctica. Two factors may have contributed to the early retreat in Maxwell Bay. First, the South Shetland Islands are located at lower latitudes, characterized by temperate conditions with frequent storms today, which should extrapolate to higher mean annual temperature, relative to Graham Land. Therefore, warmer overall temperatures may have influenced its early deglaciation. Second, Maxwell Bay is low elevation (or low orography; Turner et al., 2002) and has several outlets, with a large opening to the Bransfield Strait, where a derivative of the ACC and the Weddell Sea Transitional Water mix (Fig. 1). The configuration of Maxwell Bay, therefore, would promote influx of oceanic waters as soon as the surrounding shelf deglaciated (Heroy and Anderson, 2007).

The asynchronous onset and longevity of later Holocene climate events, such as the MHCO and the Neoglacial in the AP sites including the Palmer Deep, Collins Bay, Bigo Bay, Barilari Bay, Neny Fjord, and Maxwell Bay (Fig. 8), could be the result of several competing factors like bay physiography, the size and hypsometry of glaciers emptying into these bays, meteorological conditions and

hydrography within individual glacial drainage basins—both at the surface and in the deep ocean—especially the relatively warm CDW that may interact with the grounding zone of outlet glaciers. Allen and colleagues concluded that the Mid Holocene warmth and glacial retreat in Neny Fjord was due in large part to the influx of CDW into the southern AP continental shelf (2010). Allen and colleagues highlighted the association of *F. kerguelensis* with CDW (2010), and these oceanic diatoms are also prominent in Collins Bay throughout the Mid Holocene (Fig. 5). Christ and colleagues hypothesized that an absence of the warm CDW in Barilari Bay contributed to ice-shelf advance during the LIA (2015), and we have similar conclusions about the presence and absence of CDW being the key driver of the stability of Trooz Glacier throughout the Holocene. Therefore, multiple factors contributed to the observed changes in the stability and long-term retreat of Trooz Glacier during the Holocene.

With CDW underscored as the primary driver of glacial retreat in the western AP in recent decades (Cook et al., 2016), and a decades-long rapid warming event in the AP of five times the global mean temperature rise (from the 1950's to late 1990's; Houghton et al., 2001; Turner et al., 2002; Turner et al., 2005), there is critical need in the glacial community to characterize the long-term impacts of climate events and oceanographic changes so that we can more accurately predict the contribution of the West Antarctic Ice Sheet to future sea-level rise.

Our results indicate that while impinging warm CDW may have been a key forcing on Trooz Glacier stability during the Holocene, the large glacial drainage basin and more extensive floating ice cover, effectively reducing the surface area exposed per volume, may account for its apparent stability from the 1950's to 1990's (Cook et al., 2014), relative to other restricted bays and fjords with smaller, already receded glaciers. Oceanographic forcing is currently causing widespread retreat of glaciers in the southern AP, which are directly in contact with the water mass and the effect of CDW has been recorded in these areas (Jenkins and Jacobs, 2008; Cook et al., 2016). CDW impinges onto the West Antarctic continental shelf and melts the ice front and has hastened the retreat of several glacial systems during the Holocene (Minzoni et al., 2017; Hillenbrand et al., 2017), and has even been linked to El Nino/La Nina cycles that led to dramatic ice-shelf loss in recent years (Smith et al., 2017). With a new knowledge of the Holocene glacial retreat in Collins Bay when CDW was present, we raise concern for the future stability of Trooz Glacier, as its relatively extensive floating ice terminus may be exposed to basal melting by warm CDW today.

5. Conclusions

A 10,000-yr sediment core archive in Collins Bay, Antarctica reveals a complex history of glacial retreat and environmental changes driven by several controls, and incursion of relatively warm Circumpolar Deep Water (CDW) was an important, and perhaps dominant, forcing on the stability of Trooz Glacier during the Holocene. The combined multi-proxy analysis, including grain size, MS, density, pebble count, %TN, %TOC, $\delta^{15}N$, $\delta^{13}C$, diatom abundance and assemblage, was used to interpret glacial history, sea-ice extent, ocean productivity, and the influence of CDW on Trooz Glacier.

Trooz Glacier retreated from Collins Bay by 10,000 cal yr B.P. The sedimentary record, characterized by high MS, density and stable isotopic values, low productivity and the *Eucampia antarctica*-dominant diatom assemblage, suggests proximal glacial marine conditions during the Early Holocene, with an ice tongue or ice canopy present until 8933 cal yr B.P. An increase in productivity and diatom abundance during the glacial recession from 8933 to 6110 cal yr B.P. suggests seasonally open marine conditions and glacial retreat from outer Collins Bay. The presence of the oceanic diatom *Fragilariopsis kerguelensis* strongly suggests that CDW flowed into Collins Bay and influenced its retreat during the Early and Mid Holocene. Prominent warm marine conditions characterized Collins Bay from 6110 to 5537 cal yr B.P., as indicated by turbidites in the outer bay, low productivity and low diatom abundance. A subsequent increase in productivity and diatom abundance and the *Thalassiosira antarctica*-dominant assemblage indicates an open marine setting during the Mid-Holocene Climatic Optimum from 5537 to 3645 cal yr B.P., associated with a warm climate and possibly also due to the incursion of CDW. This was followed by cool conditions of the Late Holocene Neoglacial, which appears to have been expressed much earlier (3645 cal yr B.P.) in Collins Bay than elsewhere in the western AP, likely due to absence of CDW in the bay at that time accompanied by gradually cooling atmospheric conditions. A sharp decrease in TOC and TN, coupled with *Fragilariopsis*-prominent diatom assemblage, indicates increased sea-ice formation in the outer bay and ice-tongue/ice-canopy advance in the inner bay from 763 to 242 cal yr B.P. which corresponds with the Little Ice Age. The ice tongue/canopy then receded to its present-day position, perhaps due to warming and CDW melting the Trooz Glacier ice front.

The multi-proxy dataset suggests that the initial deglaciation of Collins Bay occurred before other bays and fjords in the AP due to its open geometry and sensitivity to warm CDW, but a floating ice canopy lingered in the bay long after the other bays became ice-free, suggesting that the large glacial drainage basin of Trooz Glacier also influenced its response to ocean forcing and climate events. While timing of initial deglaciation (from 14100 to 5742 cal yr B.P.; Milliken et al., 2009; Hardin, 2011) and expression of the Mid Holocene Climatic Optimum (with onset from 9070 to 4800 cal yr B.P.; Domack et al., 2001; Hardin, 2011) varied widely in different basins of the western AP, the Late Holocene events were fairly synchronous, with the Little Ice Age being more synchronous than any prior event in the Holocene (with onset from 763 to 380 cal yr B.P.; this study; Minzoni et al., 2015).

Several competing factors influenced the post-glacial behavior of the western AP glaciers, including the size and hypsometry of glaciers, meteorological conditions within individual glacial drainage basins, bay physiography, climate, and oceanographic conditions. As glaciers receded to the inner shelf and became smaller and more isolated during the Holocene, the widespread climate events and incursion of CDW may have become more dominant forcings on glacial stability, leading to synchronous behavior. Most of the glacial retreat observed in the western AP over recent decades has been attributed to the recent rapid warming event from the 1950's to the 1990's (Cook et al., 2014) and to >100-m water depth ocean temperatures associated with modified CDW in the southern and western AP shelf as well as the northeast AP from 1945 to 2009 C.E. (Cook et al., 2016). It is important to note that Trooz Glacier is not as small as many of the AP glaciers and may not be fully deglaciated from its inner drainage basin, accounting for its relative stability in modern time. Noting that Trooz Glacier began to retreat at its terminus in the mid 1990's, we raise concern for its future response to CDW influence, since past retreat events in Collins Bay are associated with oceanographic influence. We need to understand the relative and combined influence of these forcings on AP outlet glaciers, especially the only two glaciers that have advanced during the recent rapid warming, so that we may predict the future response of West Antarctic glaciers to climate change and CDW incursion.

Author statement

All authors contributed intellectually to this manuscript:

Conceptualization, RLT, JSW, and JBA; Methodology, RLT, ANRF, YPM, TT, AAL; Validation, RLT, JSW, TT, ANRF; Formal Analysis, ANRF, YPM, RLT, AAL; Writing- original draft preparation, RLT, ANRF; Writing-reviewing and editing, RLT, JSW, JBA, TT, YPM, AAL. All authors have agreed to submit this work to JQSR.

Data statement

All proxy data from Collins Bay will be available through the NOAA Paleoclimatology Database (https://www.ncdc.noaa.gov/data-access/paleoclimatology-data) upon publication.

Declaration of competing interest

The authors declare that they have no known competing financial interests or personal relationships that could have appeared to influence the work reported in this paper.

Acknowledgments

Collection of cores and seismic was funded by the National Science Foundation Office of Polar Programs grant ANT-0739596 to JSW and JBA and completed with funding from The University of Alabama to ANRF and RLT, as well as from the NSF Graduate Research Fellowship Program to YPM. We thank the crew and scientific party of the *RV/IB Nathaniel B. Palmer* during the NBP0703 cruise. Samples and MSCL data used were provided by the Antarctic Research Facility at Florida State University, which is now located at Oregon State University. We extend our gratitude to the staff for their assistance. We are thankful to Dr. Tony Gary and TACSWorks for use of the Fuzzy C-means software. We thank Dr. Fred Andrus for review of early drafts of the writing. We thank Dr. W. Joe Lambert and the Alabama Stable Isotope Laboratory for assistance with sample processing. We thank two anonymous reviewers for feedback that significantly improved the manuscript.

Appendix A. Supplementary data

Supplementary data to this article can be found online at https://doi.org/10.1016/j.quascirev.2021.107279.

References

Allen, C.S., Oakes-Fretwell, L., Anderson, J.B., Hodgson, D.A., 2010. A record of Holocene glacial and oceanographic variability in Neny fjord, antarctic peninsula. Holocene 20, 551–564.
Altabet, M.A., Francois, R., 1994. Sedimentary nitrogen isotopic ratio as a recorder for surface ocean nitrate utilization. Global Biogeochem. Cycles 8, 103–116.
Armand, L.K., Crosta, X., Romero, O., Pichon, J.J., 2005. The biogeography of major diatom taxa in Southern Ocean sediments: 1. Sea ice related species. Palaeoceanogr. Palaeoclimatol. Palaeoecol. 233, 93–126.
Armand, L.K., Cornet-Barthau, V., Mosseri, J., Queguiner, B., 2008. Late summer diatom biomass and community structure on and around the naturally iron-fertilized Kerguelen Plateau in the Southern Ocean. Deep Sea Res. II 55, 677–692.
Arrigo, K.R., Worthen, D.L., Robinson, D.H., 2003. A coupled ocean-ecosystem model of the Ross Sea: 2. Iron regulation of phytoplankton taxonomic variability and primary production. J. Geophys. Res.: Oceans 108 (C7).
Barnard, A., Wellner, J., Anderson, J., 2014. Late Holocene Climate Change Recorded in Proxy Records from a Bransfield Basin Sediment Core, Antarctic Peninsula, vol. 33. Polar Research.
Bart, P.J., Anderson, J.B., 1995. Seismic record of glacial events affecting the Pacific margin of the northwestern Antarctic Peninsula. Antarct. Res. 68, 75–79.
Bentley, M.J., Anderson, J.B., 1998. Glacial and marine geological evidence for the extent of grounded ice in the Weddell Sea-antarctic peninsula region during the last glacial Maximum. Antarct. Sci. 10 (3), 307–323.
Bentley, M., Hodgson, D., Sugden, D., Roberts, S., Smith, J., Leng, M., Bryant, C., 2005. Early Holocene retreat of the George VI ice shelf, antarctic peninsula. Geology 33, 173–176.
Bentley, M.J., Hodgson, D.A., 2009. Antarctic ice sheet and climate history since the last glacial Maximum. PAGES News 17, 28–29.
Bentley, M.J., Hodgson, D.A., Smith, J.A., Cofaigh, C.O., Domack, E.W., Larter, R.D., Roberts, S.J., Brachfield, S.J., Leventer, A., Hjort, C., Hillenbrand, C.D., 2009. Mechanisms of Holocene palaeoenvironmental change in the antarctic peninsula region. Holocene 19 (1), 51–69.
Bezdek, J.C., 1987. Pattern Recognition with Fuzzy Objective Function Algorithms. New York Plenum Press, New York, p. 256.
Bezdek, J.C., Pal, S.K., 1991. Fuzzy models for pattern recognition. Methods that Search for Structures in Data. IEEE Press, New York.
Blaauw, M., Christen, J.A., 2011. Flexible paleoclimate age-depth models using an autoregressive gamma process. Bayesian Anal 6 (3), 457–474. https://doi.org/10.1214/11-BA618.
Brachfeld, S., Domack, E., Kissel, C., Laj, C., Leventer, A., Ishman, S., Gilbert, R., Camerlenghi, A., Eglinton, L.B., 2003. Holocene history of the Larsen-A Ice Shelf constrained by geomagnetic paleointensity dating. Geology 31, 749–752.
Buffen, A., Leventer, A., Rubin, A., Hutchins, T., 2007. Diatom assemblages in surface sediments of the northwestern Weddell Sea, antarctic peninsula. Mar. Micropaleontol. 62, 7–30.
Burckle, L.H., 1984. Ecology and paleoecology of the marine diatom Eucampia Antarctica (castr.) mangin. Mar. Micropaleontol. 9 (1), 77–86.
Christ, A.J., Talaia-Murray, M., Elking, N., Domack, E.W., Leventer, A., Lavoie, C., Brachfeld, S., Yoo, K., Gilbert, R., Jeong, S., Petrushak, S., Wellner, J., The Larissa Group, 2015. Late Holocene glacial advance and ice shelf growth in Barilari bay, Graham land, West Antarctic peninsula. Geol. Soc. Am. Bull. 127 (1–2), 297–315.
Coale, K.H., Wang, X., Tanner, S.J., Johnson, K.S., 2003. Phytoplankton growth and biological response to iron and zinc addition in the Ross Sea and Antarctic Circumpolar Current along 170 W. Deep Sea Res. Part II Top. Stud. Oceanogr. 50 (3–4), 635–653.
Cook, A., Fox, A., Vaughan, D., Ferrigno, J., 2005. Retreating glacier fronts on the Antarctic Peninsula over the past half-century. Science 308, 541–544.
Cook, A., Holland, P., Meredith, M., Murray, T., Luckman, A., Vaughan, D., 2016. Ocean forcing of glacier retreat in the western Antarctic Peninsula. Science 353, 283–286.
Cook, A.J., Vaughan, D.G., 2010. Overview of areal changes of the ice shelves on the Antarctic Peninsula over the past 50 years. Cryosphere 4, 77–98.
Cook, A.J., Vaughan, D.G., Luckman, A.J., Murray, T., 2014. A new Antarctic Peninsula glacier basin inventory and observed area changes since the 1940s. Antarct. Sci. 26 (6), 614–624.
Convey, P., Bindschadler, R., Di Prisco, G., Fahrbach, E., Gutt, J., Hodgson, D.A., Mayewski, P.A., Summerhayes, C., Turner, J., Consortium, A., 2009. Antarctic climate change and the environment. Antarct. Sci. 21, 541–563.
Conway, T.M., Hoffmann, L.J., Breitharth, E., Strzepek, R.F., Wolff, E.W., 2016. The growth response of two diatom species to atmospheric dust from the Last Glacial Maximum. PLoS One 11 (7), e0158553.
Crosta, X., Romero, O.E., Armand, L.K., Pichon, J.-J., 2005. The biogeography of major diatom taxa in Southern Ocean surface sediments: 2. Open-ocean related species. Palaeogeogr. Palaeoclimatol. Palaeoecol. 223, 66–92.
Cunningham, W.L., Leventer, A., 1998. Diatom assemblages in surface sediments of the Ross Sea: relationship to present oceanographic conditions. Antarct. Sci. 10, 134–146.
Domack, E.W., Ishman, S.E., Stein, A.B., Mcclennen, C.E., Jull, A.J.T., 1995. Late Holocene advance of the Müller Ice Shelf, Antarctic Peninsula: Sedimentological, geochemical and palaeontological evidence. Antarct. Sci. 7 (2), 159–170.
Domack, E.W., Leventer, A., Dunbar, R., Taylor, F., Brachfeld, S., Sjunneskog, C., 2001. Chronology of the Palmer Deep site, Antarctic Peninsula: A Holocene palaeoenvironmental reference for the circum-Antarctic. Holocene 11, 1–9.
Domack, E.W., Leventer, A., Root, S., Ring, J., Williams, E., Carlson, D., Hirshorn, E., Wright, W., Gilbert, R., Burr, G., 2003. Marine Sedimentary Record of Natural Environmental Variability and Recent Warming in the Antarctic Peninsula. Antarctic Peninsula climate variability: historical and paleoenvironmental perspectives, pp. 205–224.
Domack, E., Duran, D., Leventer, A., Ishman, S., Doane, S., Mccallum, S., Amblas, D., Ring, J., Gilbert, R., Prentice, M., 2005. Stability of the Larsen B Ice Shelf on the Antarctic Peninsula during the Holocene epoch. Nature 436, 681–685.
Etourneau, J., Squbin, G., Crosta, X., Swingedouw, D., Willmott, V., Barbara, L., Houssais, M.N., Schouten, S., Damste, J.S.S., Goosse, H., Escutia, C., 2019. Ocean temperature impact on ice shelf extent in the eastern Antarctic Peninsula. Nat. Commun. 10 (1), 1–8.
Francois, R., Altabet, M.A., Burckle, L.H., 1992. Glacial-interglacial changes in surface nitrate utilization in the Indian sector of the Southern Ocean as recorded by sediment δ^{15}N. Paleoceanography 7, 589–606.
Fretwell, P., Pritchard, H.D., Vaughan, D.G., Bamber, J.L., Barrand, N.E., Bell, R., Bianchi, C., Bingham, R.G., Blankenship, D.D., Casassa, G., Catania, G., Callens, D., Conway, H., Cook, A.J., Corr, H.F.J., Damaske, D., Damm, V., Ferraccioli, F., Forsberg, R., Fujita, S., Gim, Y., Gogineni, P., Griggs, J.A., Hindmarsh, R.C.A., Holmlund, P., Holt, J.W., Jacobel, R.W., Jenkins, A., Jokat, W., Jordan, T., King, E.C., Kohler, J., Krabill, W., Riger-Kusk, M., Langley, K.A., Leitchenkov, G., Leuschen, C., Luyendyk, B.P., Matsuoka, K., Mouginot, J., Nitsche, F.O., Nogi, Y., Nost, O.A., Popov, S.V., Rignot, E., Rippin, D.M., Rivera, A., Roberts, J., Ross, N., Siegert, M.J., Smith, A.M., Steinhage, D., Studinger, M., Sun, B., Tinto, B.K., Welch, B.C., Wilson, D., Young, D.A., Xiangbin, C., Zirizzotti, A., 2013. Bedmap2: improved ice bed, surface and thickness datasets for Antarctica. Cryosphere 7, 375–393.
Garrison, D.L., Buck, K.R., Fryxell, G.A., 1987. Algal assemblages in Antarctic pack ice and in ice-edge plankton. J. Phycol. 23 (4), 564–572.
Garrison, D.L., 1991. Antarctic sea ice biota. Am. Zool. 31, 17–33.

Gary, A.C., Wakefield, M.I., Johnson, G.W., Ekhart, D.D., 2009. Application of fuzzy c-means clustering to paleoenvironmental analysis: example from the Jurassic, Central North Sea. *UK. Soc. Sediment. Geol.* Special Publ. 93, 9–20.
Gerringa, L.J., Alderkamp, A.C., Laan, P., Thuroczy, C.E., De Baar, H.J., Mills, M.M., Van Dijken, G.L., Van Haren, H., Arrigo, K.R., 2012. Iron from melting glaciers fuels the phytoplankton blooms in Amundsen Sea (Southern Ocean): iron biogeochemistry. Deep Sea Res. Part II Top. Stud. Oceanogr. 71, 16–31.
Gersonde, R., Crosta, X., Abelmann, A., Armand, L., 2005. Sea-surface temperature and sea ice distribution of the Southern Ocean at the EPILOG Last Glacial Maximum—a circum-Antarctic view based on siliceous microfossil records. Quat. Sci. Rev. 24, 869–896.
Gilbert, R., Domack, E.W., 2003. Sedimentary record of disintegrating ice shelves in a warming climate, Antarctic Peninsula. G-cubed 4.
Griffith, T.W., Anderson, J.B., 1989. Climatic control on sedimentation in bays and fjords of the northern Antarctic Peninsula. Mar. Geol. 85, 181–204.
Grove, J.M., Switsur, R., 1994. Glacial geological evidence for the medieval warm period. In the medieval warm period. Climatic Change 26, 143–169.
Harris, D., Horwáth, W.R., Van Kessel, C., 2001. Acid fumigation of soils to remove carbonates prior to total organic carbon or carbon-13 isotopic analysis. Soil Sci. Soc. Am. J. 65, 1853–1856.
Hardin, Laurin, 2011. High-resolution Holocene Glacial-marine Sediment Facies Analysis of Beascochea Bay, Western Antarctic Peninsula. University of Houston Unpublished Masters Thesis, Antarctica.
Heaton, T., Kohler, P., Butzin, M., Bard, E., Reimer, R., Austin, W., Skinner, L., 2020. Marine20—the marine radiocarbon age calibration curve (0–55,000 cal BP). Radiocarbon 62 (4), 779–820. https://doi.org/10.1017/RDC.2020.68.
Hellmer, H.H., Kauker, F., Timmermann, R., Determann, J., Rae, J., 2012. Twenty-first-century warming of a large Antarctic ice-shelf cavity by a redirected coastal current. Nature 485, 225.
Heroy, D.C., Anderson, J.B., 2005. Ice-sheet extent of the antarctic peninsula region during the last glacial Maximum (LGM)—insights from glacial geomorphology. Geol. Soc. Am. Bull. 117, 1497–1512.
Heroy, D.C., Anderson, J.B., 2007. Radiocarbon constraints on antarctic peninsula ice sheet retreat following the last glacial Maximum (LGM). Quat. Sci. Rev. 26, 3286–3297.
Hillenbrand, C.D., Smith, J.A., Hodell, D.A., Greaves, M., Poole, C.R., Kender, S., Williams, M., Andersen, T.J., Jernas, P.E., Elderfield, H., Klages, J.P., Roberts, S.J., Gohl, K., Larter, R.D., Kuhn, G., 2017. West Antarctic Ice Sheet retreat driven by Holocene warm water incursions. Nature 547, 43.
Hillenbrand, C.D., Smith, J.A., Kuhn, G., Esper, O., Gersonde, R., Larter, R.D., Maher, B., Moreton, S.G., Shimmield, T.M., Korte, M., 2010. Age assignment of a diatomaceous ooze deposited in the western Amundsen Sea embayment after the last glacial Maximum. J. Quat. Sci. 25, 280–295.
Hodgson, D.A., Bentley, M.J., Roberts, S.J., Smith, J.A., Sugden, D.E., Domack, E.W., 2006. Examining Holocene stability of antarctic peninsula ice shelves. Eos, Transactions American Geophysical Union 87, 305–308.
Hofmann, E.E., Klinck, J.M., Lascara, C.M., Smith, D.A., 1996. Water mass distribution and circulation west of the Antarctic Peninsula and including Bransfield Strait. Foundations for ecological research west of the Antarctic Peninsula 70, 61–80.
Hogan, K.A., Larter, R.D., Graham, A.G.C., Arthern, R., Kirkham, J.D., Totten Minzoni, R., Jordan, T.A., Clark, R., Fitzgerald, V., Wahlin, A.K., Anderson, J.B., Hillenbrand, C.-D., Nitsche, F.O., Simkins, L., Smith, J.A., Gohl, K., ArndtHong, J.E.J., Wellner, J., 2020. Revealing the former bed of Thwaites Glacier using sea-floor bathymetry: implications for warm-water routing and bed controls on ice flow and buttressing. The Cryoshpere 14, 2883–2908. https://doi.org/10.5194/tc-14-2883-2020.
Houghton, J.T., Ding, Y., Griggs, D.J., et al., 2001. The Scientific Basis. Intergovernmental Panel on Climate Change. Cambridge University Press, Cambridge, p. 881.
Ingolfsson, O., Hjort, C., Berkman, P.A., Bjork, S., Colhoun, E., Goodwin, I.D., Hall, B., Hirakawa, K., Melles, M., Moller, P., Prentice, M.L., 1998. Antarctic glacial history since the Last Glacial Maximum: an overview of the record on land. Antarct. Sci. 10, 326–344.
Ishman, S.E., Domack, E.W., 1994. Oceanographic controls on benthic foraminifers from the Bellingshausen margin of the Antarctic Peninsula. Mar. Micropaleontol. 24 (2), 119–155.
Jamieson, S.R., Vieli, A., O'Cofaigh, C.O., Stokes, C.R., Livingstone, S.J., Hillenbrand, C.-D., 2014. Understanding controls on rapid ice-stream retreat during the last deglaciation of Marguerite Bay, Antarctica, using a numerical model. JGR Earth Surface 119, 247–263.
Jenkins, A., Jacobs, S., 2008. Circulation and melting beneath George VI ice shelf, Antarctica. J. Geophys. Res.: Oceans 113 (C4).
Juggins, S., 2007. C2 Version 1.5 User Guide. Software for Ecological and Palaeoecological Data Analysis and Visualisation. Newcastle University, Newcastle upon Tyne, UK, p. 73pp.
Kim, S., Yoo, K.C., Lee, J.I., Khim, B.K., Bak, Y.S., Lee, J., Domack, E.W., Christ, A.J., Yoon, H.I., 2018. Holocene paleoceanography of Bigo Bay, west Antarctic Peninsula: connections between surface water productivity and nutrient utilization and its implication for surface-deep water mass exchange. Quat. Sci. Rev. 192, 59–70.
Komada, T., Anderson, M.R., Dorfmeier, C.L., 2008. Carbonate removal from coastal sediments for the determination of organic carbon and its isotopic signatures, δ13C and Δ14C: comparison of fumigation and direct acidification by hydrochloric acid. Limnol Oceanogr. Methods 6, 254–262.
Koppes, M., Hallet, B., Rignot, E., Mouginot, J., Wellner, J.S., Boldt, K., 2015. Observed latitudinal variations in erosion as a function of glacier dynamics. Nature 526, 100.
Lamb, H.H., 1965. The early medieval warm epoch and its sequel. Palaeogeogr. Palaeoclimatol. Palaeoecol. 1, 13–37.
Larter, R.D., Anderson, J.B., Graham, A.G.C., Gohl, K., Hillenbrand, C.-D., Jakobsson, M., Johnson, J.S., Kuhn, G., Nitsche, F.O., Smith, J.A., Witus, A.E., Bentley, M.J., Dowdeswell, J.A., Ehrmann, W., Klages, J.P., Lindow, J., O'cofaigh, C., Spiegel, C., 2014. Reconstruction of changes in the Amundsen Sea and Bellingshausen Sea sector of the west antarctic ice sheet since the last glacial Maximum. Quat. Sci. Rev. 100, 55–86.
Larter, R.D., Barker, P.F., 1989. Seismic stratigraphy of the Antarctic Peninsula Pacific margin: a record of Pliocene-Pleistocene ice volume and paleoclimate. Geology 17 (8), 731–734.
Larter, R.D., Cunningham, A.P., 1993. The depositional pattern and distribution of glacial-interglacial sequences on the Antarctic Peninsula Pacific margin. Mar. Geol. 109 (3–4), 203–219.
Lavoie, C., Domack, E., Pettit, E., Scambos, T., Larter, R., Schenke, H.-W., Yoo, K., Gutt, J., Wellner, J., Canals, M., 2015. Configuration of the northern antarctic peninsula ice sheet at LGM based on a new synthesis of seabed imagery. Cryosphere 9, 613–629.
Leventer, A., Domack, E.W., Ishman, S.E., Brachfeld, S., Mcclennen, C.E., Manley, P., 1996. Productivity cycles of 200–300 years in the Antarctic Peninsula region: understanding linkages among the sun, atmosphere, oceans, sea ice, and biota. Geol. Soc. Am. Bull. 108 (12), 1626–1644.
Leventer, A., Dunbar, R.B., 1996. Factors influencing the distribution of diatoms and other algae in the Ross Sea. J. Geophys. Res. 101, 18489–18500.
Leventer, A., Domack, E., Barkoukis, A., Mcandrews, B., Murray, J., 2002. Lamination from the palmer deep: a diatom-based interpretation. Paleoceanography 17 (3), 8002.
Lüning, S., Galka, M., Vahrenholt, F., 2019. The medieval climate anomaly in Antarctica. Palaeogeogr. Palaeoclimatol. Palaeoecol. 532, 109251.
Maddison, E.J., Pike, J., Leventer, A., Domack, E.W., 2005. Deglacial seasonal and subseasonal diatom record from Palmer Deep, Antarctica. J. Quat. Sci. 20 (5), 435–446.
Martinson, D.G., Stammerjohn, S.E., Iannuzzi, R.A., Smith, R.C., Vernet, M., 2008. Western Antarctic Peninsula physical oceanography and spatio–temporal variability. Deep Sea Res. Part II Top. Stud. Oceanogr. 55 (18–19), 1964–1987.
Majewski, W., Wellner, J.S., Szczucinski, W., Anderson, J.B., 2012. Holocene oceanographic and glacial changes recorded in Maxwell Bay, West Antarctica. Mar. Geol. 326, 67–79.
McCave, I., Bryant, R., Cook, H., Coughanowr, C., 1986. Evaluation of a laser-diffraction-size analyzer for use with natural sediments. J. Sediment. Res. 56.
Michalchuk, B.R., Anderson, J.B., Wellner, J.S., Manley, P.L., Majewski, W., Bohaty, S., 2009. Holocene climate and glacial history of the northeastern Antarctic Peninsula: the marine sedimentary record from a long SHALDRIL core. Quat. Sci. Rev. 28 (27–28), 3049–3065.
Milliken, K.T., Anderson, J.B., Wellner, J.S., Bohaty, S.M., Manley, P.L., 2009. High resolution Holocene climate record from Maxwell bay, South Shetland islands, Antarctica. Geol. Soc. Am. Bull. 121, 1711–1725.
Minzoni, R.T., 2015. The Antarctic Peninsula's Response to Holocene Climate Variability: Controls on Glacial Stability and Implications for Future Change. Doctoral dissertation. Rice University, Houston, TX.
Minzoni, R.T., Anderson, J.B., Fernandez, R., Wellner, J.S., 2015. Marine record of Holocene climate, ocean, and cryosphere interactions: Herbert Sound, James Ross island, Antarctica. Quat. Sci. Rev. 129, 239–259.
Minzoni, R.T., Majewski, W., Anderson, J.B., Yokoyama, Y., Fernandez, R., Jakobsson, M., 2017. Oceanographic influences on the stability of the cosgrove ice shelf, Antarctica. Holocene 27, 1645–1658.
Moffat, C., Owens, B., Beardsley, R.C., 2009. On the characteristics of Circumpolar Deep Water intrusions to the west Antarctic Peninsula continental shelf. J. Geophys. Res.: Oceans 114 (C5).
Morris, E.M., Vaughan, D.G., 2003. Spatial and temporal variation of surface temperature on the Antarctic Peninsula and the limit of viability of ice shelves. Antarct. Res. 79, 61–68.
Mulvaney, R., Abram, N.J., Hindmarsh, R.C.A., Arrowsmith, C., Fleet, L., Triest, J., Sime, L.C., Alemany, O., Foord, S., 2012. Recent Antarctic Peninsula warming relative to Holocene climate and ice-shelf history. Nature 489, 141.
Munoz, Y.P., 2018. Analysis of the sedimentary and geomorphic signature of retreating tidewater glaciers in Western Antarctic Peninsula bays (Unpublished doctoral dissertation). University of Houston, Houston, TX.
Munoz, Y.P., Wellner, J.S., 2018. Seafloor geomorphology of western Antarctic Peninsula bays: a signature of ice flow behaviour. Cryosphere 12, 205–225.
Pike, J., Allen, C.S., Leventer, A., Stickley, C.E., Pudsey, C.J., 2008. Comparison of contemporary and fossil diatom assemblages from the western Antarctic Peninsula shelf. Mar. Micropaleontol. 67 (3–4), 274–287.
Pike, J., Crosta, X., Maddison, E.J., Stickley, C.E., Denis, D., Barbara, L., Renssen, H., 2009. Observations on the relationship between the Antarctic coastal diatoms *Thalassiosira antarctica* Comber and *Porosira glacialis* (Grunow) Jørgensen and sea ice concentrations during the late Quaternary. Mar. Micropaleontol. 73, 14–25.
O'Cofaigh, C., Davies, B.J., Livingstone, S.J., Smith, J.A., Johnson, J.S., Hocking, E.P., Hodgson, D.A., Anderson, J.B., Bentley, M.J., Canals, M., 2014. Reconstruction of ice-sheet changes in the antarctic peninsula since the last glacial Maximum. Quat. Sci. Rev. 100, 87–110.
Peck, V.L., Allen, C.S., Kender, S., Mcclymont, E.L., Hodgson, D.A., 2015.

Oceanographic variability on the West Antarctic Peninsula during the Holocene and the influence of upper circumpolar deep water. Quat. Sci. Rev. 119, 54–65.
Pritchard, H., Ligtenberg, S., Fricker, H., Vaughan, D., Van den Broeke, M., Padman, L., 2012. Antarctic ice-sheet loss driven by basal melting of ice shelves. Nature 484, 502.
Pudsey, C.J., Evans, J., 2001. First survey of Antarctic sub–ice shelf sediments reveals mid-Holocene ice shelf retreat. Geology 29, 787–790.
Rebesco, M., Larter, R.D., Barker, P.F., Camerlenghi, A., Vanneste, L.E., 1997. The history of sedimentation on the continental rise west of the Antarctic Peninsula. Geology and seismic stratigraphy of the Antarctic margin 2 (71), 29–49.
Reynolds, J.M., 1981. The distribution of mean annual temperatures in the Antarctic Peninsula. Br. Antarct. Surv. Bull. 54, 123–133.
Scambos, T., Fricker, H.A., Liu, C.-C., Bohlander, J., Fastook, J., Sargent, A., Massom, R., Wu, A.-M., 2009. Ice shelf disintegration by plate bending and hydro-fracture: satellite observations and model results of the 2008 Wilkins ice shelf break-ups. Earth Planet Sci. Lett. 280, 51–60.
Scambos, T., Hulbe, C., Fahnestock, M., 2003. Climate-Induced Ice Shelf Disintegration in the Antarctic Peninsula.
Scherer, R.P., 1994. A new method for the determination of absolute abundance of diatoms and other silt-sized sedimentary particles. J. Paleolimnol. 12, 171–179.
Scott, P., Mcminn, A., Hosie, G., 1994. Physical parameters influencing diatom community structure in eastern Antarctic sea ice. Polar Biol. 14, 507–517.
Shevenell, A.E., Domack, E.W., Kernan, G.M., 1996. Record of Holocene palaeoclimate change along the Antarctic Peninsula: evidence from glacial marine sediments, Lallemand Fjord. Pap. Proc. R. Soc. Tasman. 130 (2), 55–64.
Shevenell, A.E., Ingalls, A.E., Domack, E.W., Kelly, C., 2011. Holocene Southern Ocean surface temperature variability west of the antarctic peninsula. Nature 470 (7333), 250–254.
Shipboard Scientific Party, 2007. RV/IB Nathaniel B. Palmer 2007, cruise 3 report. Collaborative Research: Controls on Sediment Yield from Tidewater Glaciers from Patagonia to Antarctica. NSF and the Antarctic Research Facility Florida State University.
Simms, A.R., Ivins, E.R., Dewitt, R., Kouremenos, P., Simkins, M., 2012. Timing of the most recent Neoglacial advance and retreat in the South Shetland Islands, Antarctic Peninsula: insights from raised beaches and Holocene uplift rates. Quat. Sci. Rev. 47, 41–55.
Smith, R.C., Ainley, D., Baker, K., Domack, E., Emslie, S., Fraser, B., Kennett, J., Leventer, A., Mosley-Thompson, E., Stammerjohn, S., 1999a. Marine ecosystem sensitivity to climate change: historical observations and paleoecological records reveal ecological transitions in the Antarctic Peninsula region. Bioscience 49, 393–404.
Smith, J., Andersen, T., Shortt, M., Gaffney, A., Truffer, M., Stanton, T., Bindschadler, R., Dutrieux, P., Jenkins, A., Hillenbrand, C.D., Ehrmann, W., F J Corr, H., Farley, N., Crowhurst, S., Vaughan, D., 2017. Sub-ice-shelf sediments record history of twentieth-century retreat of Pine Island Glacier. Nature 541, 77.
Smith, R.T., Anderson, J.B., 2010. Ice-sheet evolution in James Ross Basin, Weddell Sea margin of the Antarctic Peninsula: the seismic stratigraphic record. GSA Bull 122 (5–6), 830–842. https://doi.org/10.1130/B26486.1.
Smith, D.A., Hofmann, E.E., Klinck, J.M., Lascara, C.M., 1999b. Hydrography and circulation of the west Antarctic Peninsula continental shelf. Deep Sea Res. Oceanogr. Res. Pap. 46 (6), 925–949.
Smith, D.A., Klinck, J.M., 2002. Water properties on the west Antarctic Peninsula continental shelf: a model study of effects of surface fluxes and sea ice. Deep Sea Res. Part II Top. Stud. Oceanogr. 49 (21), 4863–4886.
Stenni, B., Curran, M.A., Abram, N., Orsi, A., Coursad, S., Masson-Delmotte, V., Neukom, R., Goosse, H., Divine, D., Van Ommen, T., Steig, E.J., 2017. Antarctic climate variability on regional and continental scales over the last 2000 years. Clim. Past 13, 1609–1634.
Stickley, C.E., Pike, J., Leventer, A., Dunbar, R., Domack, E.W., Brachfield, S., Manley, P., Mcclennan, C., 2005. Deglacial ocean and climate seasonality in laminated diatom sediments, Mac. Robertson Shelf, Antarctica. Palaeogeogr. Palaeoclimatol. Palaeoecol. 227 (4), 290–310.
Stuiver, M., Reimer, P.J., 1993. Extended 14C data base and revised CALIB 3.0 14C age calibration program. Radiocarbon 35 (1), 215–230. https://doi.org/10.1017/S0033822200013904.
Stuiver, M., Reimer, P.J., Reimer, R.W., 2021. CALIB 8.2 [WWW program] at. http://calib.org. (Accessed 7 October 2021).
Taylor, F., Mcminn, A., Franklin, D., 1997. Distribution of diatoms in surface sediments of Prydz Bay, Antarctica. Mar. Micropaleontol. 32, 209–229.
Taylor, F., Whitehead, J., Domack, E., 2001. Holocene paleoclimate change in the Antarctic Peninsula: evidence from the diatom, sedimentary and geochemical record. Mar. Micropaleontol. 41 (1–2), 25–43.
Taylor, F., Sjunneskog, C., 2002. Postglacial marine diatom record of the Palmer deep, Antarctic Peninsula (ODP Leg 178, site 1098) 2. Diatom assemblages. Paleoceanography 17 (3), 1026.
Thomas, E.R., Van Wessem, J.M., Roberts, J., Isaksson, E., Schlosser, E., Fudge, T.J., Vallelonga, P., Medley, B., Lenaerts, J., Bertler, N., Van den Broeke, M.R., Dixon, D.A., Frezzotti, M., Stenni, B., Curran, M., Ekayin, A.A., 2017. Regional Antarctic snow accumulation over the past 1000 years. Clim. Past 13, 1491–1513. https://doi.org/10.5194/cp-13-1491-2017.
Truesdale, R.S., Kellogg, T.B., 1979. Ross Sea diatoms: modern assemblage distributions and their relationship to ecologic, oceanographic and sedimentary conditions. Mar. Micropaleontol. 4, 13–31.
Turner, J., Colwell, S.R., Marshall, G.J., Lachlan-Cope, T.A., Carleton, A.M., Jones, P.D., Lagun, V., Reid, P.A., Iagovkina, S., 2005. Antarctic climate change during the last 50 years. Int. J. Climatol. 25, 279–294.
Turner, J., King, J.C., Lachlan-Cope, T.A., Jones, P.D., 2002. Climate change (Communication arising): recent temperature trends in the Antarctic. Nature 418, 291.
Turner, J., Lu, H., White, I., King, J.C., Phillips, T., Hosking, J.S., Bracegirdle, T.J., Marshall, G.J., Mulvaney, R., Deb, P., 2016. Absence of 21st century warming on Antarctic Peninsula consistent with natural variability. Nature 535 (7612), 411–415.
Vaughan, D.G., Comiso, J.C., Allison, I., Carrasco, J., Kaser, G., Kwok, R., Mote, P., Murray, T., Paul, F., Ren, J., 2013. Observations: cryosphere. Climate change 2103, 317–382.
Vaughan, D.G., Marshall, G.J., Connolley, W.M., Parkinson, C., Mulvaney, R., Hodgson, D.A., King, J.C., Pudsey, C.J., Turner, J., 2003. Recent rapid regional climate warming on the Antarctic Peninsula. Climatic Change 60, 243–274.
Wahlin, A.K., Graham, A.G.C., Hogan, K.A., Quest, B.Y., Boehme, L., Larter, R.D., Petit, E.C., Wellner, J., Heywood, K.J., 2021. Pathways and modification of warm water flowing beneath Thwaites Ice Shelf, West Antarctica. Sci. Adv. 7 (15). https://doi.org/10.1126/sciadv.abd7254.
Walker, D.P., Brandon, M.A., Jenkins, A., Allen, J.T., Dowdeswell, J.A., Evans, J., 2007. Oceanic heat transport onto the Amundsen Sea shelf through a submarine glacial trough. Geophys. Res. Lett. 34.
Warnock, J.P., Scherer, R.P., 2015. A revised method for determining the absolute abundance of diatoms. J. Paleolimnol. 53, 157–163.
Wellner, J., Heroy, D., Anderson, J., 2006. The death mask of the Antarctic ice sheet: comparison of glacial geomorphic features across the continental shelf. Geomorphology 75, 157–171.
Wellner, J.S., Scambos, T., Domack, E.W., Vernet, M., Leventer, A., Balco, G., Brachfeld, S., Cape, M.R., Huber, B., Ishman, S., Mccormick, M.L., 2019. The Larsen ice shelf system, Antarctica (LARISSA): polar systems bound together, changing fast. GSA Today (Geol. Soc. Am.) 29 (8).
Wentworth, C.K., 1922. A scale of grade and class terms for clastic sediments. J. Geol. 30 (5), 377–392.
Zielinski, U., Gersonde, R., 1997. Diatom distribution in Southern Ocean surface sediments (Atlantic sector): implications for paleoenvironmental reconstructions. Palaeogeogr. Palaeoclimatol. Palaeoecol. 129, 213–250.